Sequence-dependent cargo recognition by SNX-BARs mediates retromer-independent transport of CI-MPR

Boris Simonetti,[1] Chris M. Danson,[1] Kate J. Heesom,[2] and Peter J. Cullen[1]

[1]School of Biochemistry and [2]Proteomics Facility, School of Biochemistry, University of Bristol, Bristol, England, UK

Endosomal recycling of transmembrane proteins requires sequence-dependent recognition of motifs present within their intracellular cytosolic domains. In this study, we have reexamined the role of retromer in the sequence-dependent endosome-to–trans-Golgi network (TGN) transport of the cation-independent mannose 6-phosphate receptor (CI-MPR). Although the knockdown or knockout of retromer does not perturb CI-MPR transport, the targeting of the retromer-linked sorting nexin (SNX)–Bin, Amphiphysin, and Rvs (BAR) proteins leads to a pronounced defect in CI-MPR endosome-to-TGN transport. The retromer-linked SNX-BAR proteins comprise heterodimeric combinations of SNX1 or SNX2 with SNX5 or SNX6 and serve to regulate the biogenesis of tubular endosomal sorting profiles. We establish that SNX5 and SNX6 associate with the CI-MPR through recognition of a specific WLM endosome-to-TGN sorting motif. From validating the CI-MPR dependency of SNX1/2–SNX5/6 tubular profile formation, we provide a mechanism for coupling sequence-dependent cargo recognition with the biogenesis of tubular profiles required for endosome-to-TGN transport. Therefore, the data presented in this study reappraise retromer's role in CI-MPR transport.

Introduction

Endosomes are the major sorting compartments along the endocytic pathway. Hundreds of integral membrane proteins and their associated proteins and lipids (together termed "cargo") gather in endosomes after arriving from the plasma membrane, the biosynthetic pathway, and various other membrane trafficking routes (Huotari and Helenius, 2011; Burd and Cullen, 2014). Within endosomes, two principal decisions are made that determine cargo fate. Cargo may be selected for inclusion into an intraluminal vesicle that buds from the limiting endosomal membrane and, through endosomal maturation, is ultimately delivered to the lysosome for degradation (Schöneberg et al., 2017). Alternatively, cargo may be prevented from entering these intraluminal vesicles, and hence the degradative fate, by being instead selected for enrichment in endosomal "retrieval" subdomains for recycling back to the plasma membrane, the trans-Golgi network (TGN), or other specialized organelles (Burd and Cullen, 2014; Goldenring, 2015). The recycling of cargo occurs through the biogenesis of tubular profiles and tubulovesicular transport carriers that provide a high surface area/volume ratio (Maxfield and McGraw, 2004). An ancient and evolutionarily conserved family of proteins that regulate endosomal tubule biogenesis and are implicated in endosomal cargo sorting and recycling are the SNX–Bin, Amphiphysin, and Rvs (BAR; SNX-BAR) proteins, a subfamily of sorting nexins (SNXs; Carlton et al., 2004; Peters et al., 2004; Cullen, 2008; Cullen and Korswagen, 2011; Teasdale and Collins, 2012; Gallon and Cullen, 2015). All SNXs share a phosphoinositide-binding phox homology domain, whereas the SNX-BAR proteins also possess a BAR domain (Carlton et al., 2004; Peters et al., 2004; Traer et al., 2007; van Weering and Cullen, 2014). Through the BAR domain–mediated formation of homo- and heterodimers and corresponding higher-ordered helical arrays (Simunovic and Voth, 2015), SNX-BAR proteins organize the formation of spatially and biochemically discrete tubular profiles and tubulovesicular transport carriers (van Weering et al., 2012a,b; Ma et al., 2017).

A subset of SNX-BARs is linked to the retromer pathway (Cullen and Korswagen, 2011). Retromer is an evolutionarily conserved complex (Seaman et al., 1998), and in the higher metazoan it is a heterotrimer consisting of VPS26 (with two isoforms A and B expressed in humans), VPS29, and VPS35 (Haft et al., 2000; Kerr et al., 2005); hereon, the term "retromer" refers to the VPS26A/B–VPS35–VPS29 complex. Functionally, retromer is considered to be linked to a SNX-BAR membrane-remodeling complex composed of heterodimeric combinations of SNX1 or SNX2 with either SNX5, SNX6, or SNX32 (Horazdovsky et al., 1997; Carlton et al., 2004; Wassmer et al., 2007, 2009). Because SNX32 is also known as SNX6B, we have throughout the study referred to this as the SNX1/2–SNX5/6 complex.

Correspondence to Peter J. Cullen: pete.cullen@bristol.ac.uk

Abbreviations used: BAR, Bin, Amphiphysin, and Rvs; CI-MPR, cation-independent mannose 6-phosphate receptor; gRNA, guide RNA; KO, knockout; SILAC, stable isotope labeling by amino acids in cell culture; SNX, sorting nexin; STRING, Search Tool for the Retrieval of Interacting Genes/Proteins; TGN, trans-Golgi network.

The Rockefeller University Press
J. Cell Biol. Vol. 216 No. 11 3695–3712
https://doi.org/10.1083/jcb.201703015

The current model for retromer-mediated cargo sorting argues that endosome-associated retromer interacts with the intracellular cytosolic domains of cargo proteins either directly or via cargo adapters (Arighi et al., 2004; Seaman, 2004; Strochlic et al., 2007; Puthenveedu et al., 2010; Harterink et al., 2011; Temkin et al., 2011; Chen et al., 2013; Steinberg et al., 2013; Gallon et al., 2014; Lucas et al., 2016). Together with the actin-polymerizing Wiskott-Aldrich syndrome protein and SCAR homology (WASH) complex, retromer mediates the enrichment of selected cargo into a retrieval subdomain (Gomez and Billadeau, 2009; Harbour et al., 2010, 2012; Jia et al., 2012). Once cargo has been captured, retromer promotes the "handover" of cargo into SNX1/2–SNX5/6 tubular profiles and tubulovesicular transport carriers to allow their recycling to specific compartments. This model of retromer activity is also considered to apply to the retrograde recycling of the TGN-resident cation-independent mannose 6-phosphate receptor (CI-MPR). This receptor is transported from the Golgi to endosomes to deliver newly synthesized lysosomal hydrolases (Ghosh et al., 2003). To maintain iterative rounds of hydrolase delivery, the CI-MPR recycles back to the TGN (Lombardi et al., 1993; Meyer et al., 2000), a retrograde transport pathway that is considered to require the direct interaction of the CI-MPR with retromer (Arighi et al., 2004; Seaman, 2004).

Within this model, it is unclear how the biogenesis of SNX1/2–SNX5/6 tubular profiles and tubulovesicular transport carriers are coordinated with the recognition of cargo to ensure that profiles and carriers are only formed when cargo is sufficiently enriched. In this study, we show that the SNX1/2–SNX5/6 complex is involved in sequence-mediated cargo recognition and that for the CI-MPR, such sequence recognition is an important component in the biogenesis of tubular profiles and transport carriers during retrograde endosome-to-TGN trafficking. In considering this new insight into sequence-dependent cargo recognition within the retromer pathway, we reevaluate the existing model by which retromer regulates CI-MPR retrograde transport.

Results

The SNX1/2–SNX5/6 complex interacts with the CI-MPR

To date, stable isotope labeling by amino acids in cell culture (SILAC)-based proteomics has successfully been used to obtain high-resolution interactomes of retromer and has provided fundamental insight into the molecular details of retromer-mediated cargo sorting (Steinberg et al., 2013; McGough et al., 2014a,b; McMillan et al., 2016). To gain a better understanding of the role of the membrane remodeling complex in retromer-mediated cargo sorting, we applied the same SIL AC-based proteomic approach to the five retromer-linked SNX-BARs: SNX1, SNX2, SNX5, SNX6, and SNX32.

We lentivirally transduced human retinal pigment epithelial-1 (RPE-1) cells with increasing titers of lentivirus to generate cell populations expressing endosome-associated GFP-tagged forms of SNX1, SNX2, SNX5, SNX6, and SNX32 (Figs. S1 and S2). For the interactome analysis, we selected individual lentiviral cell lines that expressed a given GFP–SNX-BAR protein at a comparable level to the corresponding endogenous SNX-BAR protein. We were unable to confidently assess the level of GFP-SNX32 over the endogenous protein because of the lack of a reliable antibody. Therefore, we selected a viral titer where the level of GFP-SNX32 expression did not perturb the endosomal morphology (defined by excessive endosomal tubulation and endosomal vacuolation). The selected GFP–SNX-BAR–expressing cell lines were cultured in media containing amino acids of "medium" mass (R6K4), and in parallel, GFP-only expressing cells were maintained in media containing amino acids of "light" mass (R0K0). After six doublings, cells were lysed, and the lysates were immunoprecipitated using GFP-trap beads. The precipitates were combined and resolved with SDS-PAGE before liquid chromatography–tandem mass spectrometry for identification of the enriched proteins (Fig. 1 A). Data from two independent experiments were generated for each SNX-BAR protein.

For each SNX-BAR proteomic dataset, a final list of interactors was generated by excluding proteins quantified through a single unique peptide and by excluding those proteins that were not present in both duplicate experiments. The filtered lists from the two experiments were then combined, averaged, and any protein that was less than fivefold enriched over the control was excluded (Fig. 1 A). With this rationale, 10 proteins were considered to form the SNX1 interactome, 12 proteins formed the SNX2 interactome, 50 proteins formed the SNX5 interactome, 60 proteins formed the SNX6 interactome, and >200 proteins the SNX32 interactome. The increased number of interactors for SNX32 may reflect our inability to precisely define the level of overexpression relative to endogenous SNX32 and hence the selection of a suitable cell line. The five datasets were combined in Venn diagrams to show unique and common hits between SNX5, SNX6, and SNX32 (Fig. 1 B) and between SNX1 and SNX2 (Fig. 1 C). In addition, we established a Venn diagram between all five SNX-BAR interactomes (Fig. 1 C). Search Tool for the Retrieval of Interacting Genes/Proteins (STRING) analysis of all the interactors confirmed the dimeric nature of SNX-BAR interactions (Wassmer et al., 2009; van Weering et al., 2012b), with SNX1 and SNX2 forming homodimers or heterodimers with SNX5, SNX6, or SNX32 (Fig. 1 D). Known SNX-BAR–interacting partners were identified by the bioinformatics analysis. Among these, the WASH-associated protein RME-8 (also known as DNAJC13) was unique to SNX1 (Popoff et al., 2009; Shi et al., 2009; Freeman et al., 2014; Norris et al., 2017), whereas the ER tether VAPB was an interactor of the SNX2 heterodimer (Dong et al., 2016). Interestingly, the VPS26A/VPS26B, VPS29, and VPS35 components of retromer were not present in the SNX-BAR interactomes, entirely consistent with the low affinity and transient interaction described between the retromer and the SNX1/2–SNX5/6 heterodimeric complex (Collins et al., 2005).

We next used expression of GFP-tagged proteins and GFP trap–based coimmunoprecipitation to validate the association of the SNX-BAR proteins with interactors identified from the SILAC-based proteomics. We recapitulated that the SNX1/2–SNX5/6 complex does not associate with retromer, and we confirmed the specificity of the interaction within the SNX1/2–SNX5/6 complex through analysis of the nonretromer-linked SNX-BAR proteins SNX4 and SNX8 (Fig. 1 E; van Weering et al., 2012b). Western blotting of GFP trap–isolated SNX-BAR proteins confirmed the association between SNX2 and the ER tethers VAPA and VAPB (Fig. S3 A). SNX2 heterodimers were also detected in immunoprecipitates of the GFP-tagged VAPA/VAPB cytosolic domain (Fig. S3 B; Dong et al., 2016).

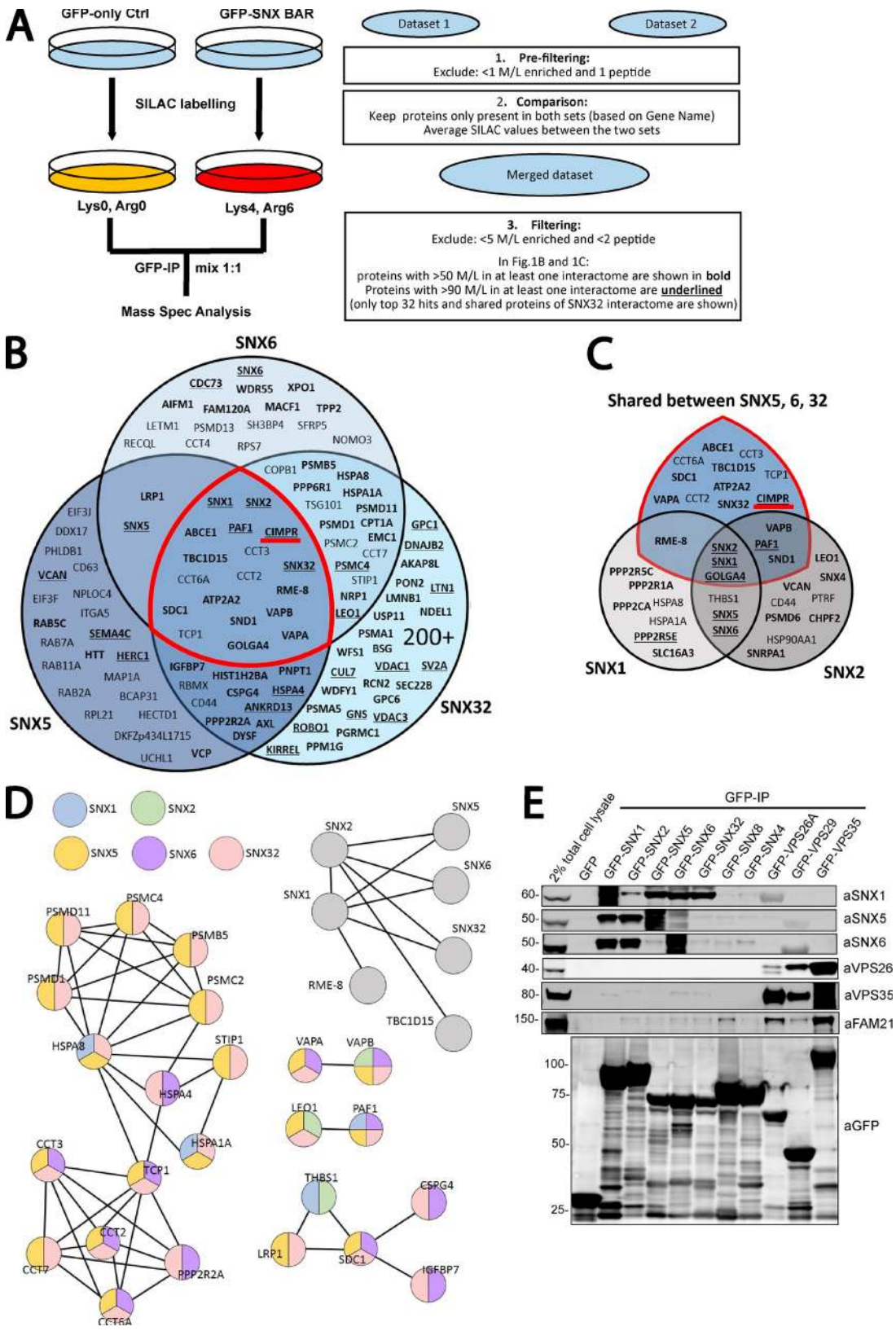

Figure 1. **Interactome of the retromer-linked SNX-BAR complex.** (A) Schematic representation of the SILAC methodology and the approach used to filter and merge SILAC datasets. (B) Venn diagram showing the interactors of SNX5, SNX6, and SNX32. (C) Venn diagram showing the interactors of SNX1 and SNX2 together with the shared interactors between SNX5, SNX6, and SNX32 (those within the red demarcated area in B). (D) STRING analysis of SNX-BAR interactors. Interactors were compiled and subjected to STRING analysis. Each connecting line represents an interaction indicated by experimental or database evidence. Color of the node indicates presence of the protein in a specific subset of the SNX-BAR interactome. (E) GFP trap of GFP-tagged retromer-linked SNX-BARs, retromer, and the retromer-independent SNX4 and SNX8, each transiently transfected in HEK293T cells. Molecular masses are given in kilodaltons. IP, immunoprecipitation.

Collectively, these data provide an initial validation of the interactome data, thereby supporting our experimental design.

Given the apparent validity of the interactome data, our attention was drawn to the high enrichment of the CI-MPR in the SNX5, SNX6, and SNX32 interactomes (Fig. 1 B). We used expression of GFP-tagged proteins in HEK293T cells followed by GFP trap–based coimmunoprecipitation to compare the binding of retromer and the SNX1/2–SNX5/6 proteins to the CI-MPR. Consistent with the SILAC-based proteomics, GFP-tagged SNX5, SNX6, and SNX32 were able to pulldown CI-MPR, whereas the interaction between retromer and the CI-MPR was not detectable (Fig. 2 A). When GFP-SNX1 or GFP-SNX2 were coexpressed with mCherry-tagged SNX5, conditions that favor the formation of SNX1–SNX5 and SNX2–SNX5 heterodimers (Wassmer et al., 2009), GFP trap immunoprecipitation revealed an enhanced association with the CI-MPR when compared with the single expression of GFP-SNX1 or GFP-SNX2, conditions that favor SNX1–SNX1 and SNX2–SNX2 homodimers (Fig. 2 B; Wassmer et al., 2009). Collectively, these data point to the SNX5, SNX6, and SNX32 components of the SNX1/2–SNX5/6 complex as being primarily involved in the binding to the CI-MPR.

We next verified whether the isolated intracellular cytoplasmic tail domain of the CI-MPR (lacking its transmembrane domain) was sufficient for binding to the SNX1/2–SNX5/6 complex. In parallel, we assessed whether binding was also detected by other cargoes undergoing retrograde endosome-to-TGN trafficking, including sortilin (Kim et al., 2010) and its family member SorLA (Fjorback et al., 2012) as well as the iron transporter DMT1-II (Tabuchi et al., 2010; for a schematic of constructs, see Fig. 2 C). Only the GFP–CI-MPR tail coimmunoprecipitated endogenous SNX5 and SNX6 and their interacting partners SNX1 and SNX2 (Fig. 2 D).

The cytoplasmic tail of the CI-MPR contains a hydrophobic WLM sorting motif that is necessary for the endosome-to-TGN transport of this receptor (Seaman, 2007). Mutation of the WLM sequence motif leads to the endosomal accumulation of a CD8–CI-MPR reporter (Seaman, 2007), a phenotype that we also observed with a corresponding mutant in full-length CI-MPR (Fig. 2 E). Thus, we tested the ability of a WLM mutant CI-MPR to interact with SNX5, SNX6, and SNX32. Quantitative western analysis revealed that deletion of the WLM triplet, its mutation into AAA, or the switching of the WLM motif for the FLV endosome-to-TGN sorting motif of sortilin (Seaman, 2007) resulted in a complete loss of binding to these SNX-BAR proteins (Fig. 2 F). In contrast, a truncated form of the CI-MPR that still contained the WLM motif retained binding (Fig. 2 F). Overall, these data establish that the WLM motif in the cytosolic domain of the CI-MPR interacts with SNX1/2–SNX5/6 heterodimers, with SNX5 and SNX6 (and SNX32) being the most likely cargo binding entities.

Sequence-mediated recognition of the CI-MPR contributes to SNX1/2–SNX5/6 tubular carrier biogenesis

Immunofluorescence analysis in HeLa cells established that the bulk of endogenous CI-MPR localized to the TGN, but significant amounts were also found in perinuclear retromer-positive endosomes (Fig. 3 A). Endosomes are complex organelles that are spatially organized, with a mosaic of distinct functional subdomains whose size is below the classic resolution of light microscopy (Sönnichsen et al., 2000; Murk et al., 2003; Puthenveedu et al., 2010). Expression of a GTPase-defective Rab5 mutant, Rab5(Q79L), has been used to enlarge endosomes to discriminate between nonoverlapping domains on the endosome membrane by conventional confocal microscopy (Barbieri et al., 1996; Raiborg et al., 2002). We used this approach to investigate CI-MPR segregation in retromer-positive endosomes. We scored the overlap of the endogenous CI-MPR signal with that of endogenous VPS35 (a core retromer component) and SNX2 (a component of the SNX1/2–SNX5/6 complex) on the limiting membrane of enlarged endosomes (Fig. 3 B). Immunofluorescence analysis showed that CI-MPR was enriched in domains positive for SNX2 alone or SNX2 and VPS35 domains but was largely excluded from VPS35-only subdomains (Fig. 3 B, right). These data indicate that endosomal CI-MPR is mostly enriched in SNX1/2–SNX5/6 subdomains.

To investigate the functional role of the interaction between CI-MPR and the SNX1/2–SNX5/6 complex, we engineered a chimeric construct encoding the transmembrane domain and intracellular cytosolic domain of the CI-MPR linked to a fluorescent tag that was orientated to face the lumen (Fig. 4 A). Strikingly, the overexpression of this construct induced the formation of elongated CI-MPR–positive tubular profiles previously reported to be CI-MPR–enriched post-TGN carriers (extensively characterized by Waguri et al., 2003). However, we observed that endogenous SNX1 and SNX2 as well as SNX6 were found to localize with a subpopulation of CI-MPR–positive tubular profiles (Figs. 3 C and S4 A). When cells were costained for endogenous VPS35, we observed that retromer was excluded from the subpopulation of CI-MPR–containing SNX1/2–SNX5/6–decorated tubular profiles (Figs. 3 D and S4 A). As the SNX1/2–SNX5/6 decorated CI-MPR–containing tubular profiles were observed to emerge from VPS35-labeled endosomes, we concluded that rather than being emanations of the TGN, this subpopulation of tubular profiles constituted transport tubules emerging from endosomes (Figs. 3 E and S4 A). Consistent with this, this subpopulation of tubular profiles lacked the presence of the TGN marker TGN46 (Fig. S4 A) and was observed by live-cell imaging to undergo processes of fusion and fragmentation (Fig. S4 B and Video 1).

We next introduced the WLM-to-AAA mutation into the GFP–CI-MPR chimera (Fig. 4 A). WT GFP-CI-MPR and the WLM-to-AAA mutant had similar levels of expression, and the expression of neither construct perturbed the level of retromer pathway components (Figs. 4 B and S4 C). The WLM-to-AAA–carrying GFP–CI-MPR mutant, which we confirmed reduced the ability to bind to the SNX1/2–SNX5/6 complex (Fig. 4 C), was still observed in tubular profiles (Fig. 4 D). However, immunostaining of endogenous SNX1 to specifically highlight the endosome-derived subpopulation of CI-MPR–containing tubules revealed that although the number of SNX1-negative WT and WLM-to-AAA mutant GFP–CI-MPR tubular profiles were not significantly perturbed (Fig. 4 E), those endosomal tubular profiles that were specifically decorated with endogenous SNX1 were significantly reduced in the WLM-to-AAA mutant (Fig. 4 E). These observations are consistent with the formation of SNX1/2–SNX5/6 tubular transport profiles being dependent, in part, on the presence of the WLM endosome-to-TGN sorting motif within the intracellular cytosolic domain of the CI-MPR. Importantly, endogenous retromer was excluded from these tubular domains, suggesting that it is not a component of these CI-MPR–positive SNX1/2–SNX5/6 tubular profiles (Fig. 4 E).

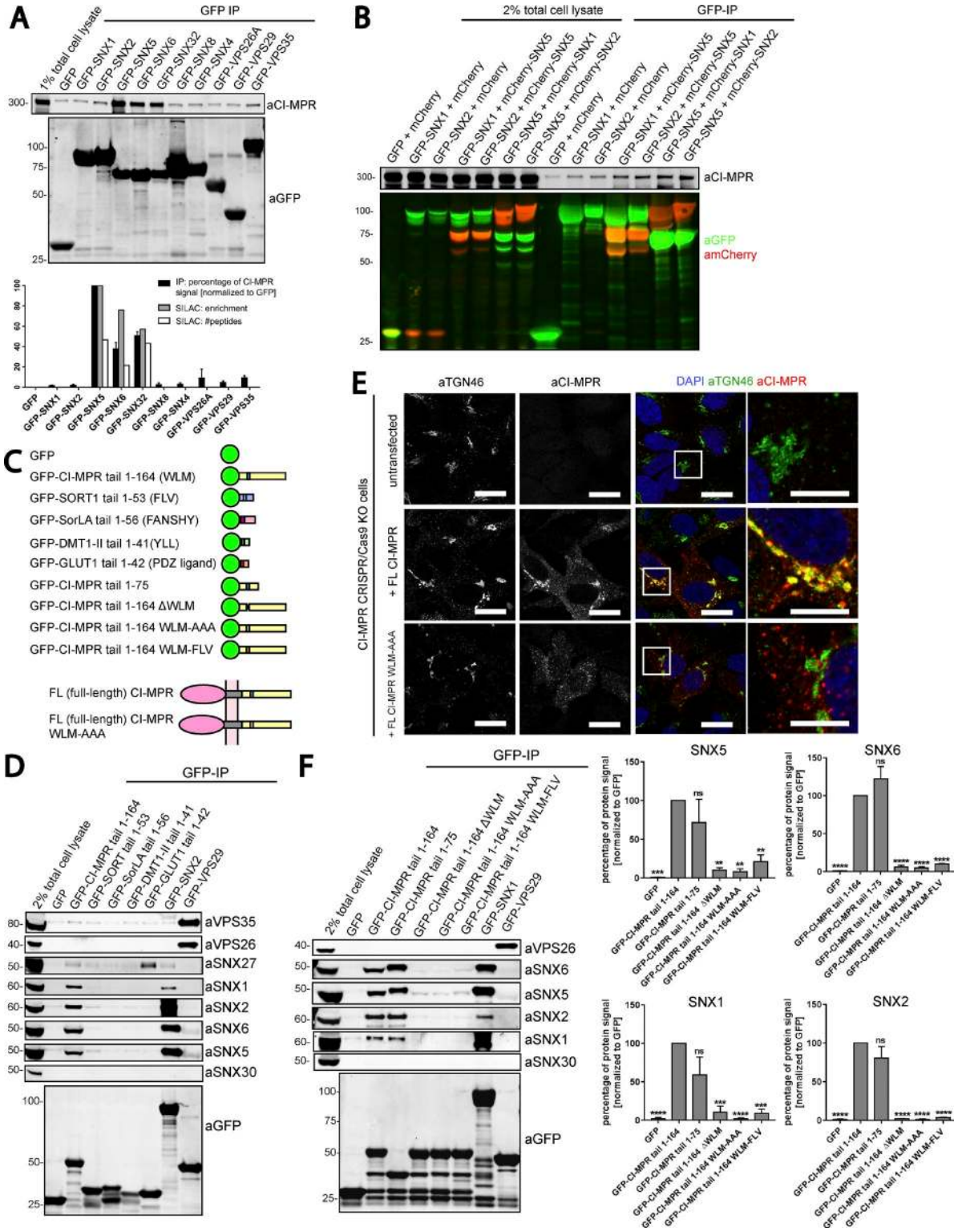

Figure 2. **SNX5, SNX6, and SNX32 interact with the CI-MPR tail via the WLM sorting motif.** (A) Consistent with SILAC-based proteomics, GFP-tagged SNX5, SNX6, and SNX32 but not SNX1, SNX2, or retromer immunoprecipitate (IP) CI-MPR in a GFP-trap experiment. Under the blots is a summary of CI-MPR binding ability from quantitative fluorescence-based Western blotting and SILAC-based enrichment and peptide counts. (B) Coexpression of heterodimeric combinations of GFP-tagged and mCherry-tagged SNX1–SNX5 and SNX2–SNX5 in HEK293T cells. GFP trap of GFP-SNX1 and GFP-SNX2 revealed an enhanced association with CI-MPR when the formation of SNX1–SNX5 and SNX2–SNX5 was favored by coexpression of the binding partner SNX5. (C) Summary of constructs used. Retrograde sorting motifs in brackets correspond with the black boxed regions. (D) GFP trap of GFP-tagged cargo tails transiently transfected in HEK293T cells showing that of the tails' constructs; only CI-MPR pulls down the retromer-linked SNX-BARs but little, if any, of the retromer. SNX30 was used as a negative control. (E) The WLM motif within the tail of CI-MPR is an endosome-to-TGN sorting motif. HeLa cells were cotransfected with CRISPR-Cas9 plasmids against CI-MPR and a puromycin resistance–expressing plasmid before puromycin selection 24 h later. Cells were then transfected with full-length (FL) CI-MPR or full-length CI-MPR WLM-AAA. 48 h after transfection, cells were incubated with an antibody targeting

The SNX1/2–SNX5/6 complex mediates the retrograde endosome-to-TGN trafficking of the CI-MPR

To define the functional importance of the binding of SNX1/2–SNX5/6 proteins to the CI-MPR and the formation of recycling tubules, we compared CI-MPR trafficking in retromer and SNX1/2–SNX5/6 siRNA knockdown cells. Owing to the fact that SNX1 and SNX2 are functionally redundant and that the same is also true for SNX5 and SNX6 (Rojas et al., 2007; Wassmer et al., 2007, 2009), we used a combination of siRNAs targeting each SNX-BAR protein. As previously reported, the suppression of SNX1/2–SNX5/6 did not affect the level of retromer (Fig. 5 A; Steinberg et al., 2013). Immunofluorescence analysis of endogenous CI-MPR localization in siRNA-treated HeLa cells showed that loss of the retromer component VPS35 had little if any effect on the steady-state distribution of the CI-MPR (Fig. 5 B). However, the loss of the SNX1/2–SNX5/6 proteins caused a pronounced shift of the CI-MPR signal from TGN to peripheral punctae, with 15% of the cells displaying a full vesicular CI-MPR distribution (Fig. 5 B). To determine the nature of these CI-MPR–containing peripheral punctae, we used immunostaining of endosomal markers. In SNX1/2–SNX5/6–suppressed cells, the CI-MPR was partially but significantly redistributed to endosomes positive for the late endosome/lysosome marker LAMP1 and the early endosome marker EEA1 but was fully redistributed to an endosomal population positive for VPS35 (Fig. 5, C and D). We also compared protein levels of the CI-MPR to determine whether the redistribution to retromer-positive endosomes correlated with enhanced lysosomal degradation. No reduction of CI-MPR protein level was observed in cells treated with siRNA oligonucleotides targeting the SNX1/2–SNX5/6 complex or the retromer (Fig. 6 A). Blocking of protein synthesis with cycloheximide treatment did not reveal an altered rate of CI-MPR turnover (Fig. 6 A), consistent with neither the SNX1/2–SNX5/6 complex nor the retromer functioning to retrieve the CI-MPR cargo away from the lysosomal degradative fate.

To assess whether the redistribution of CI-MPR was caused by an endosome-to-TGN trafficking defect, we followed the retrograde trafficking of a previously characterized CI-MPR CD8 chimera in HeLa cells (Seaman, 2007). The CD8 tag was surface exposed and hence suitable for antibody uptake experiments, and the CD8–CI-MPR showed a delayed retrograde trafficking to the TGN in SNX1/2–SNX5/6–suppressed cells, as shown by decreased Pearson colocalization with the TGN marker TGN46 after 10 and 20 min of antibody uptake (Fig. 6 B). Cells suppressed for retromer showed minor but significantly faster routing to the TGN at 10 min after internalization, suggesting that the proposed interaction between retromer and the CI-MPR is dispensable for endosome-to-TGN recycling (Fig. 6 B).

Gene editing confirms the essential role of the SNX1/2–SNX5/6 complex in the retromer-independent endosome-to-TGN transport of the CI-MPR

To exclude that the lack of an observed CI-MPR trafficking phenotype in retromer-suppressed cells arose from a partial but not complete loss of VPS35 expression, we used CRISPR-Cas9 technology to generate knockout (KO) cells. Initially, we compared the distribution of the CI-MPR in nonclonally selected cellular populations transfected with CRISPR-Cas9 vectors targeting VPS35, simultaneous SNX1 and SNX2, or SNX5 and SNX6. Western blot analyses confirmed the successful reduction of the targeted proteins in the nonclonal population; no change was detected in the total level of CI-MPR (Fig. 7 A). A crude analysis confirmed that in a subpopulation of cells targeted with either SNX1–SNX2 or SNX5–SNX6 guide RNA (gRNA) but not with gRNA against VPS35, the CI-MPR shifted its steady-state distribution from a tight juxtanuclear location (consistent with the TGN) to a more peripheral distribution (Fig. 7 A). The visualization of endogenous SNX1 and VPS35 by single-cell immunofluorescent analysis allowed the identification of KO cells within the cellular population and their internal side-by-side comparison with neighboring WT cells. In contrast to VPS35 KO cells, where the distribution of the endogenous CI-MPR was indistinguishable from that observed in WT cells, in the SNX1–SNX2 KO cells the CI-MPR was redistributed and accumulated in retromer-positive endosomes (Fig. 7 B). Single-cell quantitative analysis of nonclonal populations targeting SNX5 and SNX6 further confirmed that perturbing the SNX1/2–SNX5/6 complex led to a shift in the steady-state distribution of the CI-MPR from the TGN into EEA1-positive endosomes (Fig. 7 C).

From these nonclonal populations, we isolated clonal HeLa cell lines that were biochemically characterized as VPS35 KOs, dual SNX1 and SNX2 KOs, and dual SNX5 and SNX6 KOs (two independent lines being isolated for each condition; Fig. 8, A and B). Consistent with the network of interactions that assemble the SNX1/2–SNX5/6 complex (Wassmer et al., 2009), the SNX1–SNX2 KO cell lines displayed a clear reduction in the levels of SNX5 and SNX6, which was mirrored in the SNX5–SNX6 KO cell lines (Fig. 8 A). Likewise, in the VPS35 KO cell lines, there was a clear reduction in the levels of VPS26 and VPS29, the two other proteins that assemble with VPS35 to form the stable retromer heterotrimeric complex (Fig. 8 A; Arighi et al., 2004; Seaman, 2004). There was no evidence that the expression of the SNX1/2–SNX5/6 complex was affected in the retromer KO cell lines, nor was the expression of retromer affected upon KO of SNX1–SNX2 or SNX5–SNX6 (Fig. 8 A). In all of these clonal HeLa cell lines, the steady-state expression of CI-MPR was not significantly affected (Fig. 8 A).

To assess the CI-MPR distribution, we imaged each clonal cell line and quantified the colocalization of endogenous CI-MPR with TGN46 and EEA1. This confirmed the clear and statistically significant steady-state redistribution of the CI-MPR from the TGN to peripheral endosomes in the SNX1–SNX2 KO cell lines and, more strikingly, in the SNX5–SNX6 KO cell lines (Fig. 8 B). We again failed to observe any significant redistribution of the CI-MPR in the VPS35 KO cell lines (Fig. 8 B). However, a feature of the isolated VPS35 KO clones was a "fragmented" TGN (Fig. 8 B). Finally, to ensure that the observed CI-MPR phenotype did not arise from off-target effects, we individually reexpressed GFP-SNX5 and GFP-SNX6 in the

the CI-MPR extracellular domain, and its trafficking was analyzed after 40 min. Zoomed images on right are marked by boxes in main images. Bars: (main images) 20 µm; (zooms) 10 µm. (F) The CI-MPR WLM sorting motif is necessary for interaction with the retromer-linked SNX-BARs. Summary of CI-MPR mutant binding ability from quantitative fluorescence–based Western blotting. SNX30 was used as negative control. $n = 3$ independent experiments (means ± SEM; one-way ANOVA compared with GFP–CI-MPR tail 1–164. *, $P < 0.05$; **, $P < 0.01$; ***, $P < 0.001$; ****, $P < 0.0001$).

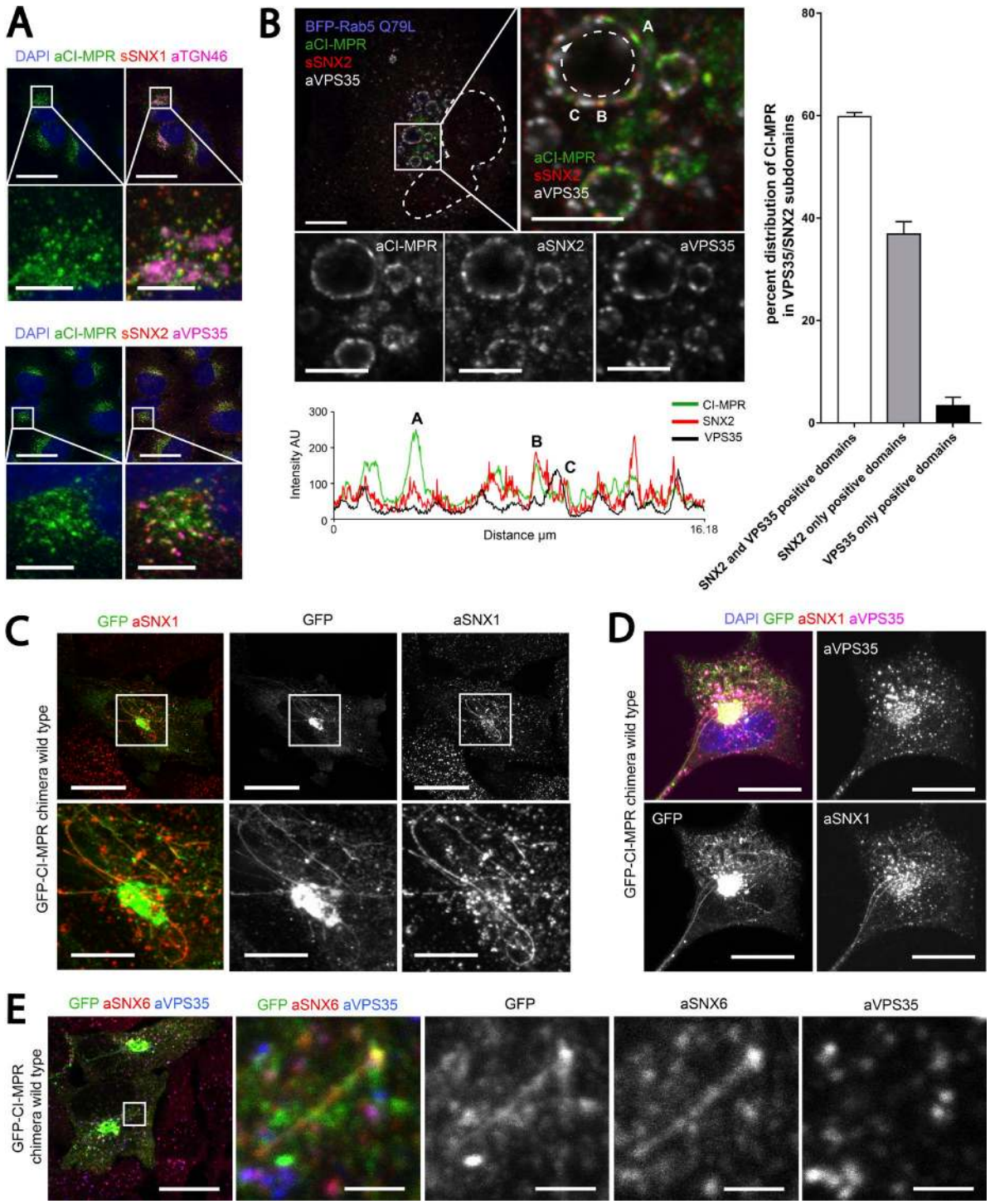

Figure 3. **CI-MPR segregates in SNX1/2–SNX5/6 tubular profiles which are not decorated with retromer.** (A) Endogenous CI-MPR localizes to a highly packed vesicular cluster that colocalized with the TGN and partially colocalized with retromer-positive endosomes. HeLa cells were fixed and immunostained for endogenous TGN46 (TGN marker), VPS35 (retromer), SNX1, and SNX2 (both retromer-linked SNX-BARs). Bars: (main images) 20 µm; (zooms) 5 µm. (B, top) CI-MPR colocalizes with SNX2-positive subdomains on enlarged endosomes. HeLa cells were transfected with BFP-Rab5Q79L and immunostained for endogenous CI-MPR, SNX2, and VPS35 after 48 h. The dashed line in the top left image indicates the contour of the nucleus, and the dashed line on the top right refers to the enlarged endosome from which the intensity line scan was measured. Bars: (main images) 10 µm; (zooms) 5 µm. (B, bottom) Line scan of signal intensity across the circumference of enlarged endosome. (B, right) Distribution of CI-MPR in retromer subdomains; $n = 3$ independent experiments. CI-MPR signal was quantified in 36 enlarged endosomes (means ± SEM). (C) Overexpression of a WT GFP–CI-MPR chimera leads to the formation of extended CI-MPR tubules, some of which are positive for endogenous SNX1. HeLa cells were transfected with GFP–CI-MPR chimera WT and immunostained for SNX1 after 48 h. Bars: (main images) 20 µm; (zooms) 10 µm. (D) A subpopulation of GFP–CI-MPR chimera tubules is decorated with endogenous SNX1 but not endogenous VPS35. HeLa cells were transfected with GFP–CI-MPR chimera WT and immunostained for SNX1 and VPS35 after 48 h. Bars, 20 µm. (E) Some SNX1/2–SNX5/6-decorated CI-MPR–containing tubules were observed to emanate from VPS35-positive endosomes. HeLa cells were transfected with GFP–CI-MPR chimera WT and immunostained for SNX6 and VPS35 after 48 h. The box in the leftmost panel indicates the area depicted in the other four panels. Bars: (main images) 20 µm; (zooms) 2 µm.

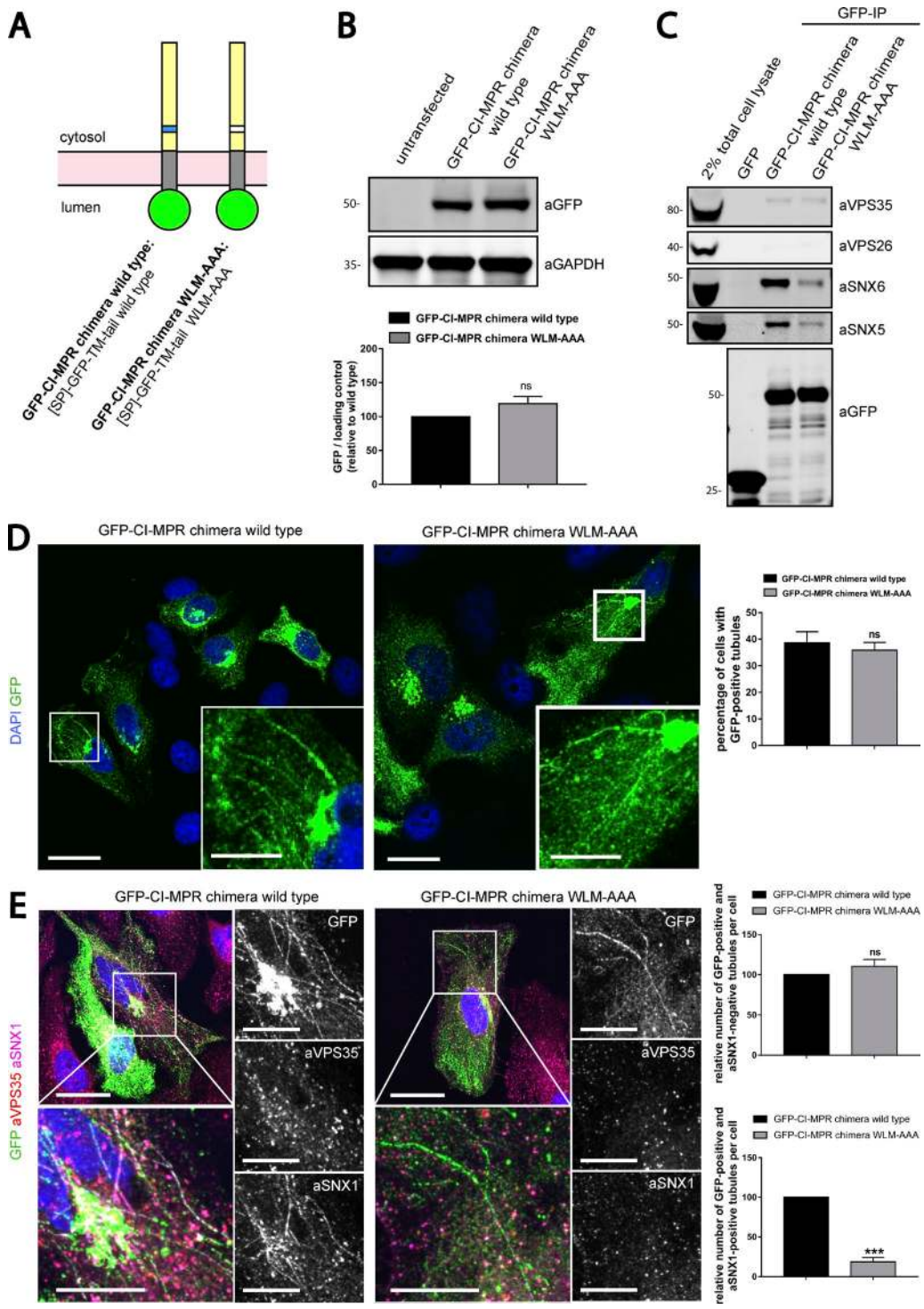

Figure 4. **SNX1 is less efficiently recruited to CI-MPR tubules expressing a chimera harboring the WLM-AAA mutation.** (A) Scheme of CI-MPR chimera constructs used. SP, signal peptide; TM, transmembrane domain. (B, top) The GFP–CI-MPR chimera WT and the GFP–CI-MPR chimera WLM-AAA mutant have comparable expression levels. HeLa cells were transfected with CI-MPR chimeras. 48 h after transfection, GFP levels were analyzed by Western blotting. (B, bottom) $n = 3$ independent experiments. (C) The GFP–CI-MPR chimera WLM-AAA mutant has a reduced ability to bind to the SNX1/2–SNX5/6 complex. GFP trap of GFP-tagged GFP–CI-MPR chimeras, each transiently transfected in HEK293T cells. Molecular masses are given in kilodaltons. IP, immunoprecipitation. (D, left) HeLa cells were transfected with WT or WLM-AAA mutant GFP–CI-MPR chimera constructs. Bars: (main images) 20 µm; (insets) 5 µm. (D, right) The percentages of cells with at least one GFP-positive tubule were blindly scored. $n = 3$ independent experiments; WT, 145 cells; WLM-AAA, 139 cells. (E) HeLa cells were transfected with WT or WLM-AAA mutant GFP–CI-MPR construct and immunostained for endogenous SNX1 and endogenous VPS35 after 48 h. Bars: (main images) 20 µm; (insets) 10 µm. (E, top right) Relative number of GFP-positive and SNX1-negative tubules per cell. $n = 3$ blindly scored independent experiments; WT, 40 cells; WLM-AAA, 38 cells. (E, bottom right) Relative number of GFP-positive and SNX1-positive tubules per cell. $n = 3$ blindly scored independent experiments; WT, 40 cells; WLM-AAA, 38 cells (means ± SEM; unpaired *t* test; *, $P < 0.05$; ***, $P < 0.001$). The total number of tubules analyzed in WT cells was 254 tubules and in WLM-AAA cells was 199 tubules.

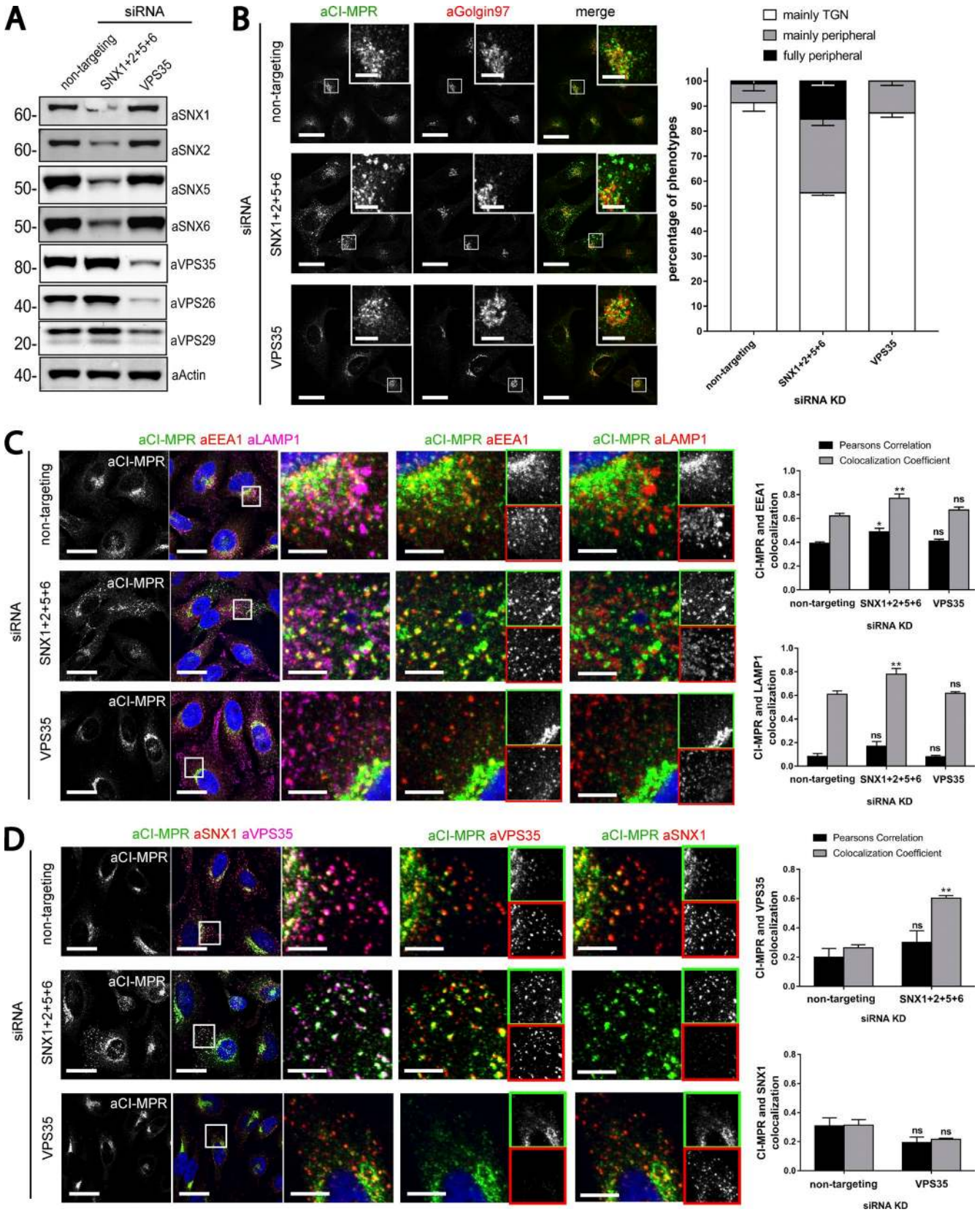

Figure 5. **Loss of the SNX1/2–SNX5/6 complex leads to an accumulation of CI-MPR in endosomes.** (A) HeLa cells were transiently transfected with nontargeting siRNA, siRNA targeting VPS35 or an siRNA pool against SNX1, SNX2, SNX5, and SNX6. 72 h after transfection, endogenous protein levels were analyzed by Western blotting. (B) CI-MPR steady-state localization in retromer versus retromer-linked SNX-BAR–knockdown cells. Representative images (left) and blind scoring and quantification (right) of the percentage of cells displaying each phenotype in knockdown conditions. $n = 3$ independent experiments; nontargeting, 144 cells; SNX1+2+5+6, 169 cells; VPS35, 133 cells. (C) Immunofluorescence and colocalization analysis of endogenous CI-MPR

SNX5–SNX6 KO cell lines (Figs. 9 A and S5). Expression of either protein rescued the normal steady-state distribution of the CI-MPR (Figs. 9 A and S5). This phenotypic rescue was not observed upon expression of either GFP-SNX4 or GFP-SNX8, two SNX-BAR proteins that do not assemble into the SNX1/2–SNX5/6 complex and do not associate with the CI-MPR (Figs. 9 A and S5).

Discussion

Our data provide the conceptual framework to propose a mechanism for how the SNX1/2–SNX5/6 membrane-remodeling complex is able to couple sequence-dependent CI-MPR recognition with the biogenesis of CI-MPR–enriched tubular profiles and transport carriers during retrograde endosome-to-TGN transport. From a parallel analysis of retromer, we have provided data that challenge the current dogma for describing the functional role of retromer in sequence-dependent CI-MPR retrograde transport.

We have established that the WLM endosome-to-TGN sorting motif present within the intracellular cytoplasmic tail domain of the CI-MPR (Seaman, 2007) interacts with heterodimeric combinations of SNX5, SNX6, or SNX32 with one of SNX1 or SNX2. When reconstituted in an in vitro liposome-based assay, these SNX-BAR proteins display an inherent ability to generate tubular profiles (van Weering et al., 2012b). As peripheral proteins, SNX-BARs associate with the cytosolic face of the endosomal membrane through an avidity-based engagement that detects the presence of specific phosphoinositide species (via their phox homology domains) and senses membrane curvature through the lipid-binding properties of their BAR domains and associated amphiphatic helices (Carlton et al., 2004; Traer et al., 2007; van Weering et al., 2012b). As the local density of the SNX-BAR proteins increases, they switch from curvature-sensing to curvature-inducing modes of action, the latter arising from the formation of high-ordered helical assembles that drive the biogenesis of tubular profiles (Simunovic and Voth, 2015). Our identification that the SNX5, SNX6, and SNX32 proteins can also associate with sorting motifs in the intracellular cytosolic domain of cargo proteins as exemplified in this study by the CI-MPR argues that the density of specific cargo is an important component in the avidity-based residency of SNX-BAR proteins on the endosomal membrane. This ability to sense the concentration of cargo proteins would influence the local density of SNX-BAR proteins at regions of cargo-enrichment, thereby aiding their assembly into helical arrays that drive the localized biogenesis of tubular profiles. In this way, sequence-dependent cargo recognition is coupled to the biogenesis of the tubular profile (Fig. 9 B).

Consistent with this model, we have shown that increased expression of WT CI-MPR leads to an enhancement in the formation of SNX1/2–SNX5/6–decorated tubular profiles when compared with the WLM-AAA CI-MPR mutant that lacks binding and hence is not sensed by these SNX-BAR proteins. It is very likely, therefore, that the other cargo proteins identified within the interactomes described in this study as well as in other previously published studies (Kurten et al., 1996; Haft et al., 1998; Parks et al., 2001; Heydorn et al., 2004a,b; Villar et al., 2013) are also recognized by the SNX1/2–SNX5/6 complex to regulate their tubular-based endosomal sorting and transport. The diversity in cargo recognition between SNX1 and SNX2 and between SNX5, SNX6, and SNX32 may expand the repertoire of cargoes being selected and provide unique points of regulation for specific recycling routes. Furthermore, with a limited body of evidence hinting that other SNX-BAR proteins, including SNX8 and SNX4 as well as SNX7 and SNX30, may also display abilities to associate with cargo proteins (Haft et al., 1998; Bean et al., 2017; Ma et al., 2017), the concept of cargo recognition within SNX-BAR–mediated biogenesis of tubular profiles and cargo-enriched transport carriers is likely to extend to other transport routes. Our data also reveal that the endosome-to-TGN transport of TGN46 occurs independently of the retromer-linked SNX-BARs (and VPS35), suggesting that other endosome-to-TGN trafficking pathways contribute to the retrograde transport of this protein.

The observed redistribution of the steady-state localization of the CI-MPR upon SNX1–SNX2 and SNX5–SNX6 siRNA knockdown or CRISPR-Cas9 KO is entirely consistent with the described interaction between the SNX1/2–SNX5/6 complex and the WLM endosome-to-TGN sorting motif in the CI-MPR. Our experiments using siRNA knockdown and CRISPR-Cas9 KO argue that retromer itself plays a very minor (if any) role in regulating the steady-state distribution of the CI-MPR, a conclusion that contrasts with previous studies (Arighi et al., 2004; Seaman, 2004). These distinct functional requirements for retromer and the SNX1/2–SNX5/6 complex in CI-MPR transport are entirely consistent with the biochemical evidence that in solution, retromer and the SNX1/2–SNX5/6 complex do not associate to form a stable assembly (Norwood et al., 2011). Our unbiased proteomic analysis has provided further evidence supporting this conclusion and hence reinforced that in mammalian cells, these complexes do not appear to form a higher-ordered complex. It should not be excluded, however, that a transient association of these complexes might occur in a membrane-dependent context, which if of low affinity would not be detected through our proteomic procedure. We have also observed that although mammalian retromer and the SNX1/2–SNX5/6 complex do colocalize on shared CI-MPR–enriched endosomal subdomains, a greater proportion of these subdomains are enriched with the SNX1/2–SNX5/6 complex over retromer, again consistent with a separation of their functional properties. Thus, in contrast to yeast, where the Vps26–Vps35–Vps29 heterotrimer physically interacts with the SNX-BAR equivalents Vps5–Vps17 (Seaman et al., 1998), in higher metazoans, this is not the case.

Finally, the evidence that siRNA knockdown and CRISPR-Cas9 KO of retromer does not alter the steady-state distribution

and lysosomal marker LAMP1 and early endosomal marker EEA1 in SNX1, SNX2, SNX5, and SNX6 or VPS35-knockdown HeLa cells. (C, top right) $n = 3$ independent experiments; nontargeting, 130 cells; SNX1+2+5+6, 162 cells; VPS35, 103 cells. (C, bottom right) $n = 3$ independent experiments; nontargeting, 115 cells; SNX1+2+5+6, 131 cells; VPS35, 109 cells. (D) Immunofluorescence and colocalization analysis of endogenous CI-MPR and transition endosome markers SNX1 and VPS35 in SNX1, SNX2, SNX5, and SNX6 or VPS35-deficient HeLa cells. Bars: (main images) 20 µm; (insets) 5 µm. (D, top right) $n = 3$ independent experiments; nontargeting, 101 cells; SNX1+2+5+6, 100 cells. (D, bottom right) $n = 3$ independent experiments; nontargeting, 98 cells; VPS35, 119 cells (means ± SEM; two-way ANOVA compared with nontargeting control; *, $P < 0.05$; **, $P < 0.01$).

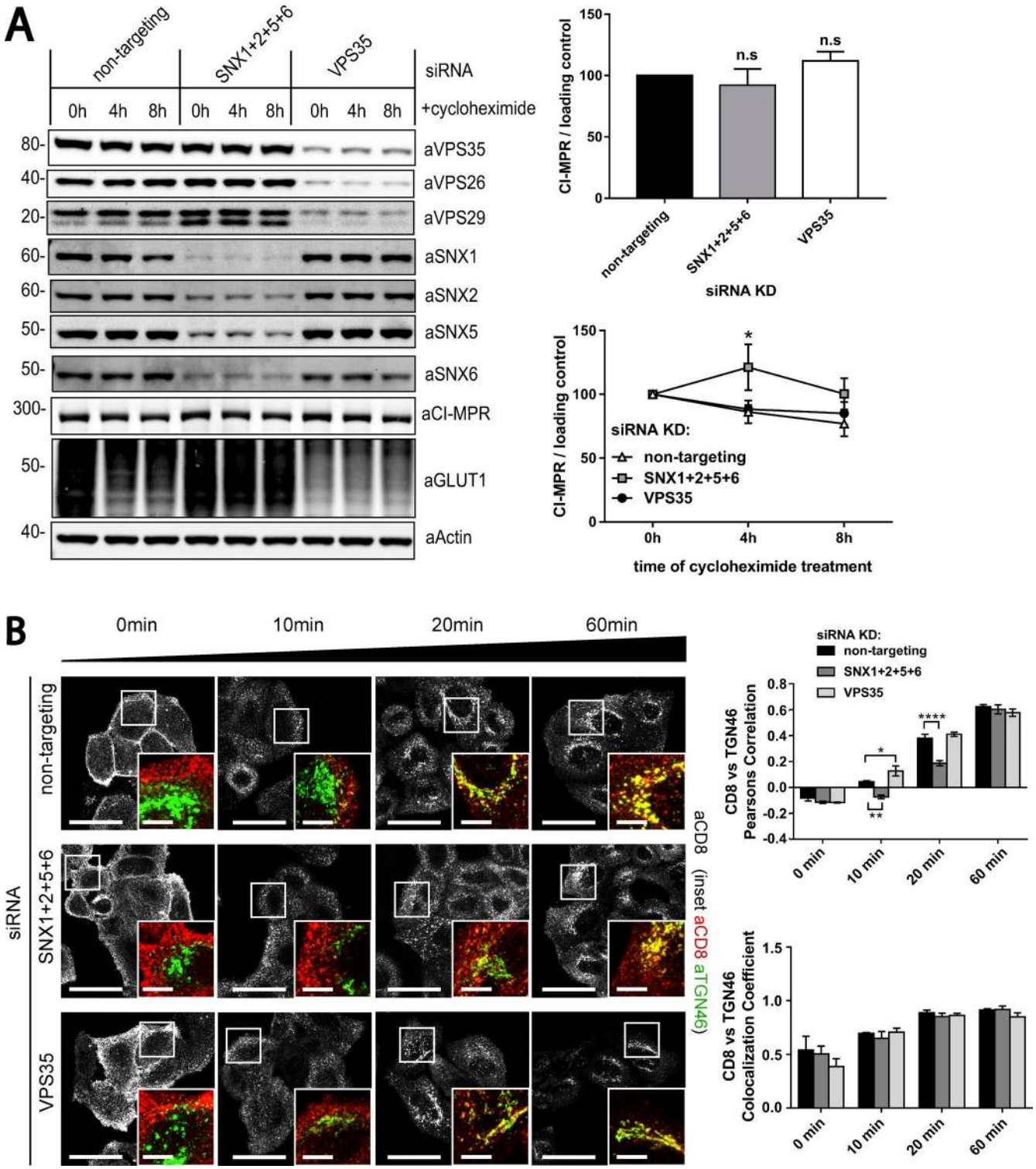

Figure 6. **Loss of the SNX1/2–SNX5/6 complex leads to a pronounced retrograde sorting defect of the CI-MPR.** (A) Degradation assay of endogenous CI-MPR. HeLa cells were transfected with nontargeting siRNA, siRNA against VPS35, or a pool of siRNAs against SNX1, SNX2, SNX5, and SNX6. 72 h after transfection, cells were incubated with 10 µg/ml cycloheximide and lysed at different time points as indicated. The level of endogenous CI-MPR was analyzed by quantitative Western blotting. Molecular masses are given in kilodaltons. (A, top right) $n = 4$ independent experiments (one-way ANOVA compared with nontargeting control). (A, bottom right) $n = 4$ independent experiments (two-way ANOVA compared with nontargeting control). (B) CI-MPR–CD8 uptake assays in retromer and retromer-linked SNX-BAR–knockdown cells show a retrograde trafficking defect only in SNX1/2–SNX5/6–depleted cells. HeLa cells were transfected with nontargeting siRNA, siRNA against VPS35, or a pool of siRNAs against SNX1, SNX2, SNX5, and SNX6. 72 h after transfection, cells were incubated with αCD8 antibody, and its trafficking was followed for 60 min. The retrograde transport to the TGN was assayed through measuring colocalization of CD8 signal with the TGN marker TGN46. $n = 3$ independent experiments; 0 min, ≥72 cells per condition; 10 min, ≥74 cells per condition; 20 min, ≥78 cells per condition; 60 min, ≥69 cells per condition (means ± SEM; two-way ANOVA compared with nontargeting control; *, $P < 0.05$; **, $P < 0.01$; ****, $P < 0.0001$). Bars: (main images) 20 µm; (insets) 5 µm.

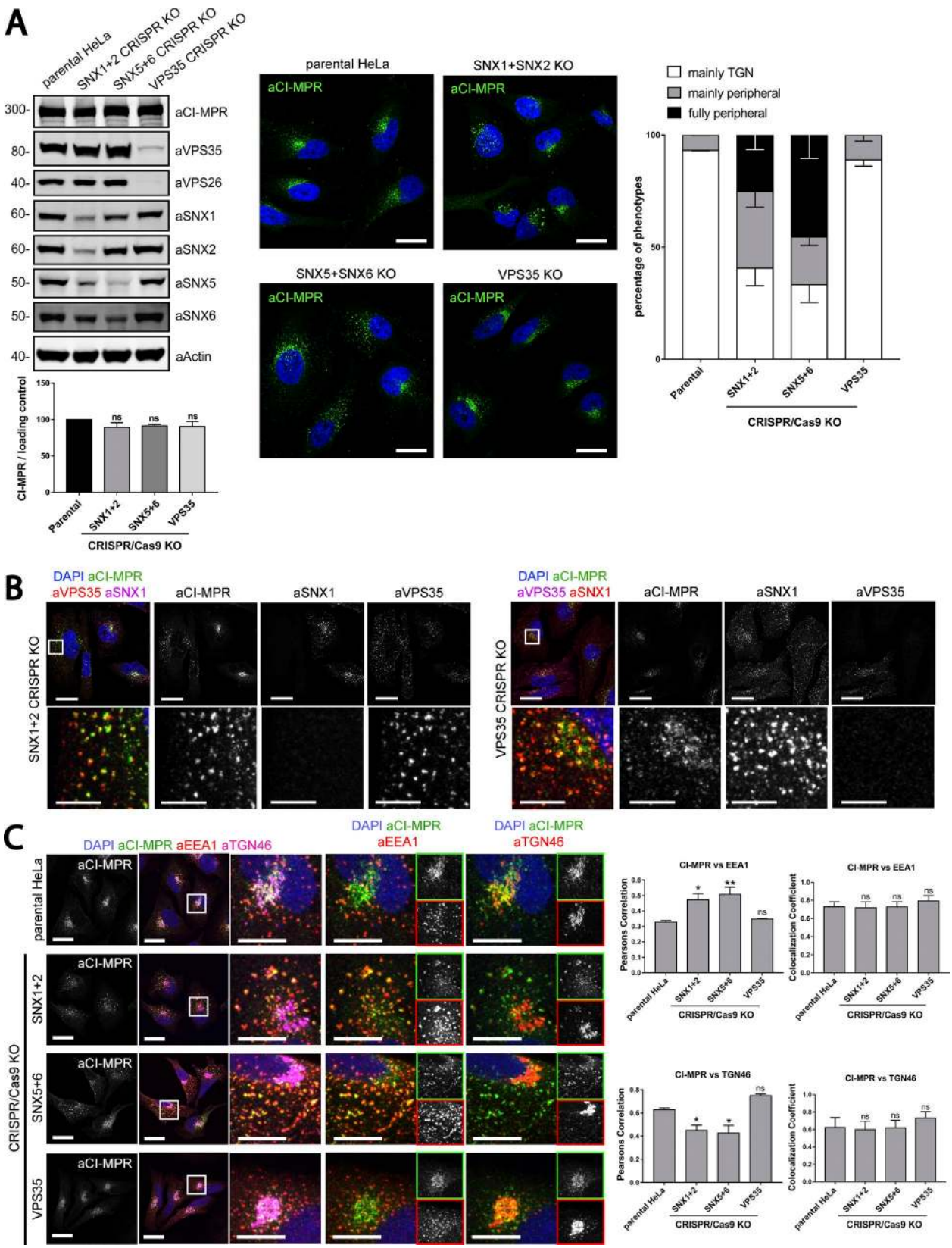

Figure 7. **Gene editing confirms the essential role of SNX1/2–SNX5/6 in endosome-to-TGN recycling of CI-MPR.** (A, left) CI-MPR levels and CI-MPR steady-state localization in retromer and SNX1/2–SNX5/6 KO cells. HeLa cells were transfected with CRISPR-Cas9 plasmids against SNX1 and SNX2, SNX5 and SNX6, or VPS35. 96 h after transfection, endogenous protein levels were analyzed by Western blotting, and cells were fixed and stained for endogenous CI-MPR. $n = 3$ independent experiments (one-way ANOVA compared with parental HeLa). Molecular masses are given in kilodaltons. (A, middle) Representative images. Bars, 20 µm. (A, right) quantification of the percentage of cells displaying each phenotype. $n = 3$ blindly scored independent experiments; parental, 116 cells; VPS35, 106 cells; SNX5 + SNX6, 111 cells; VPS35, 106 cells. (B) Immunofluorescence of endogenous CI-MPR and endogenous SNX1

of the CI-MPR is at odds with previous studies (Arighi et al., 2004; Seaman, 2004). From the data presented in our study, we conclude that the present view of retromer's role in the endosome-to-TGN retrograde transport of the CI-MPR may be overstating its direct importance in the sequence-dependent element of this transport process. Further work will be required to reconcile these differences and to define further the importance of retromer in retrograde endosome-to-TGN transport.

Materials and methods

Antibodies

Antibodies used in this study were: mouse monoclonal antibodies to SNX1 (clone 51/SNX1; 611482; BD), SNX2 (clone 13/SNX2; 5345661; BD), SNX6 (clone SNX6-76; S6324; Sigma-Aldrich), SNX6 (clone D-5,365965; Santa Cruz Biotechnology, Inc.), LAMP1 (H4A3; 25630; Abcam), GLUT1 (SPM498; 40084; Abcam), CD8 (clone UCHT4; ANC-153-020; Ancell), β-actin (A1978; Sigma-Aldrich), GFP (clones 7.1 and 13.1; 11814460001; Roche), Golgin-97 (clone CDF4; A-21270; Thermo Fisher Scientific), CI-MPR (clone 2G11; MA1-066; Thermo Fisher Scientific); rabbit polyclonal antibodies to SNX1 (ab995; Abcam), SNX5 (17918-1-AP; Proteintech), VPS26A (23892; Abcam), VPS35 (97545; Abcam), VPS29 (98929; Abcam), FAM21 (a gift from D.D. Billadeau, Mayo Clinic, Rochester, MN), Strumpellin (87442; Santa Cruz Biotechnology, Inc.), SNX30 (ab121600; Abcam), VAPB (14477-1-AP; Proteintech), SNX27 (16329-1-AP; Proteintech), GAPDH (G9545; Sigma-Aldrich); rabbit monoclonal antibodies to SNX5 (EPR14358; 180520; Abcam), VPS35 (EPR11501(B); 157220; Abcam), CI-MPR (EPR6599; 124767; Abcam), GLUT1 (EPR3915; 115730; Abcam), EEA1 (clone c45b10; 3288; Cell Signaling Technology), SNX4 (epr16954; ab198504; Abcam), goat polyclonal antibodies to VPS35 (10099; Abcam), SNX6 (N-19; Santa Cruz Biotechnology, Inc.), and EEA1 (N-19; sc-6415; Santa Cruz Biotechnology, Inc.), sheep polyclonal antibody to TGN46 (AHP500G; Bio-Rad Laboratories), and mouse polyclonal antibody to VAPA (SAB2702059; Sigma-Aldrich).

Cell culture and transfection

HeLa cells were grown in DMEM (Sigma-Aldrich) supplemented with 10% (vol/vol) FCS (Sigma-Aldrich) and penicillin/streptomycin (Gibco) and grown under standard conditions. DNA was transfected using FuGENE HD (Promega) according to the manufacturer's instructions. CRISPR-Cas9 plasmids were cotransfected with a puromycin resistance–expressing plasmid, and cells were subjected to puromycin selection 24 h later. For siRNA-based knockdown, cells were first reverse-transfected using DharmaFECT (GE Healthcare) and then transfected again with HiPerFect (QIAGEN) 24 h later according to the manufacturer's instructions. 48 h after the second transfection, cells were lysed or fixed and stained. Retromer SNX-BAR suppression was done using a combination of the following oligonucleotides against SNX1 (sequence 5′-AAGAACAAGACCAAGAGCCAC-3′), SNX2 (sequence 5′-AAGUCCAUCAUCUCCAGAACC-3′), SNX5 (sequence 5′-CUACGAAGCCCGACUUUGA-3′), and SNX6 (sequence 5′-UAAAUCAGCAGAUGGAGUA-3′). VPS35 suppression was done using a combination of oligonucleotide 3 (sequence 5′-GUUGUUAUGUGCUUAGUA-3′) and oligonucleotide 4 (sequence 5′-AAAUACCACUUGACACUUA-3′; GE Healthcare). Cycloheximide was used to prevent up-regulation of protein synthesis. In this case, cycloheximide (C7698; Sigma-Aldrich) at 10 µg/ml was added to the cells 24 h after the second transfection for the indicated time points.

Generation of lentiviral stable RPE-1 cell lines

Lentiviral particles were produced and harvested in HEK293T cells. hTERT-RPE1 cells were transduced with a titration of lentiviral particles to produce stably transduced cells. HEK293T and hTERT RPE-1 cells were grown in DMEM supplemented with 10% (vol/vol) FCS and penicillin/streptomycin and grown at 37°C in a 5% CO_2 incubator.

Isolation of CRISPR-Cas9 clonal lines

HeLa cells were grown in DMEM supplemented with 10% (vol/vol) FCS and penicillin/streptomycin and grown under standard conditions. CRISPR-Cas9 plasmids were cotransfected with a puromycin resistance–expressing plasmid using FuGENE HD according to the manufacturer's instructions, and cells were subjected to puromycin selection 24 h later. Cells were subsequently resuspended using accutase (BioLegend) and diluted in Iscov's modified Dulbecco's medium (Sigma-Aldrich) supplemented with 10% (vol/vol) FBS (Sigma-Aldrich) to 2.5 cells/ml. Subsequently, 200 µl was plated in the wells of 10× 96-well plates, and after 3 wk, the plates were screened for the presence of cell colonies. Cell colonies were expanded and subjected to lysis and Western blotting to determine the levels of the target proteins.

SILAC

For SILAC, hTERT RPE1 cells lentivirally transduced to stably express GFP or a GFP-tagged construct of the protein of interest were cultured for at least six doublings in SILAC DMEM (89985; Thermo Fisher Scientific) supplemented with 10% dialyzed FBS (F0392; Sigma-Aldrich). Cells expressing GFP were grown in media containing light amino acids (R0K0), whereas cells expressing the GFP-tagged protein of interest were grown in medium (R6K4). Amino acids R6, R0, and K0 were obtained from Sigma-Aldrich, whereas K4 was from Thermo Fisher Scientific. Cells where lysed in immunoprecipitation buffer (50 mM Tris-HCl, 0.5% NP-40, and Roche protease inhibitor cocktail) and subjected to GFP trap (ChromoTek). Precipitates were pooled and separated on NuPAGE 4–12% precast gels (Invitrogen) before liquid chromatography–tandem mass spectrometry analysis on an Orbitrap Velos mass spectrometer (Thermo Fisher Scientific).

Immunoprecipitation and quantitative Western blot analysis

For Western blotting, cells were lysed in PBS with 1% Triton X-100 and protease inhibitor cocktail. The protein concentration was determined with a BCA assay kit (Thermo Fisher Scientific), and equal amounts were resolved on NuPAGE 4–12% precast gels (Invitrogen). Blotting was performed onto polyvinylidene fluoride membranes (Immobilon-FL; EMD Millipore) followed by detection using the Odyssey infrared scanning system (LI-COR Biosciences). In using the Odyssey, we routinely performed Western blot analysis where a single blot was simultaneously probed with antibodies against two proteins of interest (distinct antibody species) followed by visualization with the corresponding secondary antibodies conjugated to distinct spectral dyes.

and VPS35 in retromer KO cells and SNX1 and SNX2 KO cells. Bars: (top) 20 µm; (bottom) 5 µm. (C) Immunofluorescence and colocalization analysis of endogenous CI-MPR and TGN marker TGN46 and early endosomal marker EEA1 in SNX1 and SNX2, SNX5 and SNX6, and VPS35 CRISPR-Cas9 KO HeLa cells. Bars: (main images) 20 µm; (insets) 10 µm. (C, top right) $n = 3$ independent experiments; parental HeLa, 80 cells; SNX1+2 KO, 99 cells; SNX5+6, 81 cells; VPS35 KO, 76 cells. (C, bottom right) $n = 4$ independent experiments; parental HeLa, 102 cells, SNX1+2 KO, 114 cells; SNX5+6, 104 cells; VPS35 KO, 102 cells (means ± SEM; one-way ANOVA compared with parental HeLa; *, $P < 0.05$; **, $P < 0.01$).

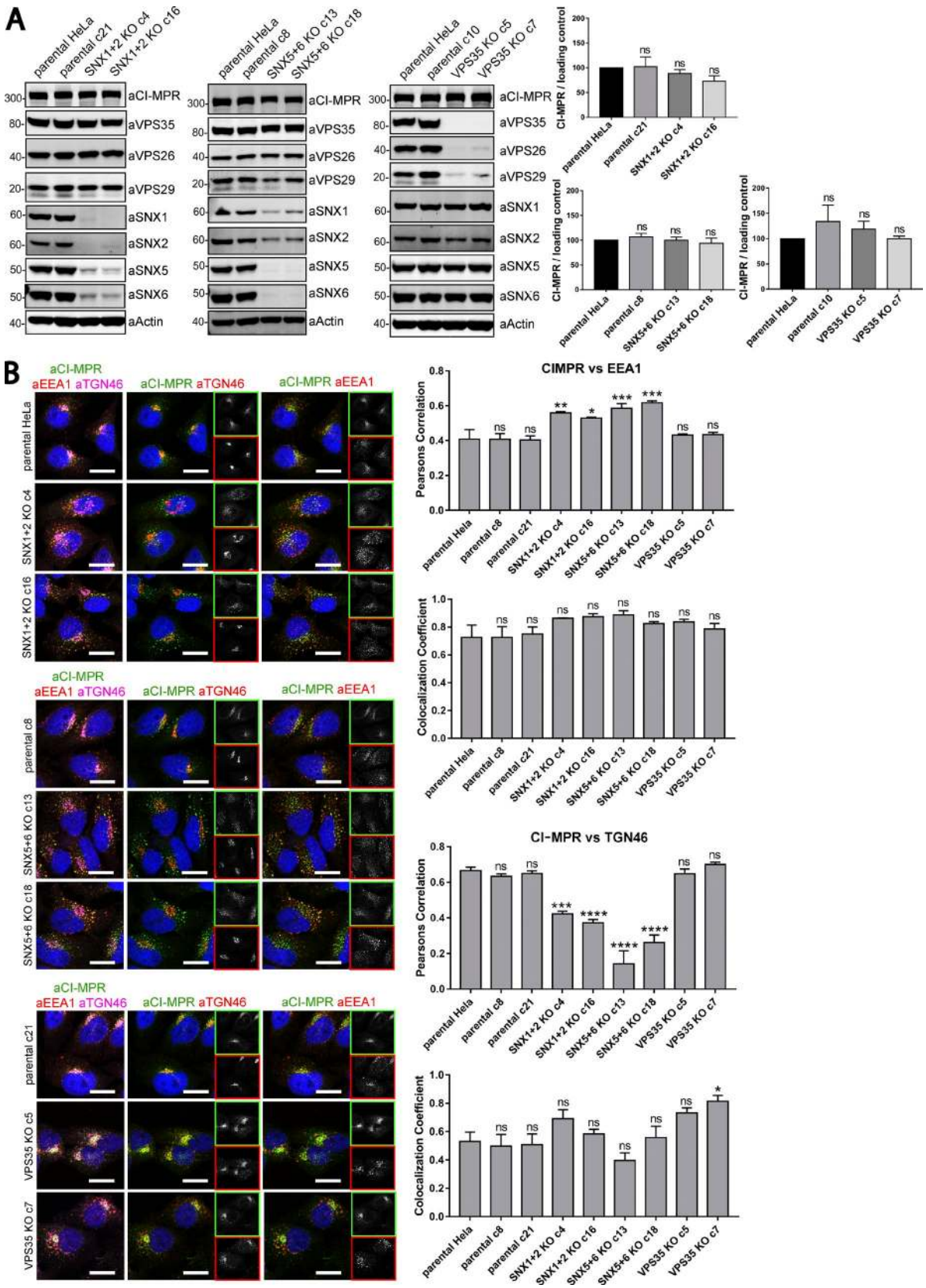

Figure 8. **Clonal HeLa KO cell lines recapitulate the SNX1/2–SNX5/6 mediated retromer-independent retrograde transport of CI-MPR.** (A) Clonal cell lines were isolated from a heterogeneous population of CRISPR-Cas9 KO. Two independent lines were biochemically characterized as SNX1+2 KOs, two as SNX5+6 KOs, two as VPS35 KOs, and three as parental clonal lines. Molecular masses are given in kilodaltons. (A, right) CI-MPR levels were analyzed by Western blotting. *n* = 3 independent experiments. (B, left) Immunofluorescence and colocalization analysis of endogenous CI-MPR, TGN marker TGN46, and early endosomal marker EEA1 in parental HeLa and clonally selected KO lines. Bars, 20 µm. (B, top right two graphs) *n* = 3 independent experiments;

For GFP-based immunoprecipitations, HEK293T cells were transfected with GFP constructs using polyethylenimine (Sigma-Aldrich). 48 h after transfection, cells were lysed in immunoprecipitation buffer (50 mM Tris-HCl, 0.5% NP-40, and Roche protease inhibitor cocktail) and subjected to GFP trap (ChromoTek).

Immunofluorescence staining

Cells were washed and fixed in 4% PFA and then washed in PBS and permeabilized with 0.1% Triton X-100. For the preservation of Rab5 Q79L swollen endosomes, cells were fixed in ice-cold methanol for 4 min. Fixed cells were then blocked in 1% BSA and incubated in primary antibody and respective secondary antibody (Alexa Fluor; Thermo Fisher Scientific) in 1% BSA. For the aCD8 antibody uptake assay, D8–CI-MPR–HeLa cells (Seaman, 2004) were transferred to a well containing 3 ml of ice-cold DHB (DMEM supplemented with 20 mM Hepes and 1% [vol/vol] FCS) for 15 min to stop trafficking processes. Surface CD8–CI-MPR was labeled by 30 min incubation in cold DHB-containing aCD8 antibody. Coverslips were washed twice in ice-cold PBS, transferred to prewarmed growth media, and returned to the incubator for 0, 10, 20, or 60 min to allow uptake of the anti-CD8 to occur. At the assay end point, cells were washed, fixed, and immunostained. Similar protocol was adopted for the CI-MPR antibody uptake assay.

Image acquisition and image analysis

Microscopy images were collected with a confocal laser-scanning microscope (SP5 AOBS; Leica Microsystems) attached to an inverted epifluorescence microscope (DMI6000; Thermo Fisher Scientific). A 63× 1.4 NA oil immersion objective (Plan Apochromat BL; Leica Biosystems) and the standard SP5 system acquisition software and detector were used. Images were captured at room temperature as z stacks with photomultiplier tube detectors with a photocathode made of gallium-arsenide-phosphide (Leica Microsystems) for collecting light emission. Images were captured using Application Suite AF software (version 2.7.3.9723; Leica Microsystems) and then analyzed with the Volocity 6.3 software (PerkinElmer). For colocalization studies, Pearson's correlation (measuring the correlation in the variation between two channels) and Manders's colocalization coefficient (measuring the degree to which the corresponding channel overlaps with the other channel) were measured using the method of Costes to set automatic thresholds. The colocalization in Fig. 5 D was measured in the cell periphery (entire cell area excluding the TGN region), and it was measured in the entire cell area in all the other cases. In Fig. 4, an individual tubular profile was scored based on a length that was ≥3 µm. Cells were seeded in dishes (MatTek) in prewarmed CO_2-independent media. Cells were imaged with a confocal laser scanning microscope (SP8 AOBS; Leica Microsystems) attached to a DMI6000 inverted epifluorescence microscope with an HCX Plan Apochromat lambda blue 63× 1.4 NA oil objective. Images were captured at 37°C, and "Adaptive Focus Control" was used to correct focus drift during time courses.

Plasmids

Cytoplasmic domain of VAPA, VAPB, CI-MPR tail, SORT1 tail, SorLA tail, DMT1-II tail, and GLUT1 tail were cloned from HeLa cDNA into pEGFPC1 vector (Takara Bio Inc.). Primers for site-directed mutagenesis of the CI-MPR tail were designed according to the online tool QuikChange Primer Design (Agilent Genomics). Signal peptide of CI-MPR and transmembrane domain and tail of CI-MPR for the generation of chimeric constructs were amplified from HeLa cDNA and cloned into pEGFPC1 vector (Takara Bio Inc.). The CRISPR-Cas9 plasmids in px330 were gifts from F. Steinberg (Albert Ludwigs Universitaet Freiburg, Freiburg, Germany). The gRNAs for CRISPR genome editing used in this study were SNX1, 5′-GGCCGGGGGATC AGAACCCG-3′; SNX2, 5′-GCAGCACTGTCTCCACCCTAG-3′; SNX5, 5′-GCTCTGAAACGTGGGCAGTG-3′; SNX6, 5′-GATGTG CTGCCACACGACAC-3′; VPS35, 5′-GTGGTGTGCAACATCCCT TG-3′; CI-MPR gRNA1, 5′-GCTTGTCCTGAGTTACGTGA-3′, CI-MPR gRNA2, 5′-GTGTGCACTACTTTGAGTGG-3′; and CI-MPR gRNA3, 5′-GAGAAGGAAGACCTCCTCTG-3′.

Statistical analysis

All quantified Western blot and confocal colocalization data are the mean of at least three independent experiments. Statistical analyses were performed using Prism 7 (GraphPad Software). Graphs represent means and SEM. The following statistical tests have been used: *t* test (unpaired and two-tailed), one-way ANOVA (followed by Dunnett's test), two-way ANOVA (followed by Dunnett's test with the exception of Fig. 5 D, in which Sidak's test was used). For all statistical tests, $P < 0.05$ was considered significant and is indicated by asterisks.

Online supplemental material

Fig. S1 shows the titration of GFP-SNX1 and GFP-SNX2 lentivirally transduced RPE1 cells as well as the endosomal localization of GFP-SNX1 and GFP-SNX2 chimeras. Fig. S2 shows the titration of GFP-SNX5, GFP-SNX6, and GFP-SNX32 lentivirally transduced RPE1 cells as well as the endosomal localization of GFP-SNX5, GFP-SNX6, and GFP-SNX32 chimeras. Fig. S3 recapitulates the interaction between VABA and SNX2 heterodimers. Fig. S4 shows that the WT GFP–CI-MPR chimera induces the formation of tubules decorated with SNX1/2–SNX5/6 complex but not with retromer. Fig. S5 shows how the rescue of CI-MPR in the SNX5+6 KO c18 by reexpression of GFP-tagged SNX5 or SNX6 rescues the normal steady-state distribution. Video 1 shows how the SXN1-decorated GFP–CI-MPR chimera tubules are highly dynamic.

Acknowledgments

We thank the Wolfson Bioimaging Facility at the University of Bristol for their support.

This work was supported by the Wellcome Trust grants 089928 and 104568 to P.J. Cullen. B. Simonetti was supported by a Wellcome Trust PhD Studentship for the Dynamic Cell Biology program (083474).

The authors declare no competing financial interests.

Submitted: 3 March 2017
Revised: 19 July 2017
Accepted: 11 August 2017

parental HeLa, 58 cells; parental c8, 79 cells; parental c21, 81 cells; SNX1+2 KO c4, 75 cells; SNX1+2 KO c16, 70 cells; SNX5+6 KO c13, 82 cells; SNX5+6 KO c18, 89 cells; VPS35 KO c5, 83 cells; VPS35 KO c7, 72 cells. (B, bottom right two graphs) *n* = 3 independent experiments; parental HeLa, 67 cells; parental c8, 72 cells; parental c21, 87 cells; SNX1+2 KO c4, 83 cells; SNX1+2 KO c16, 80 cells; SNX5+6 KO c13, 84 cells; SNX5+6 KO c18, 98 cells; VPS35 KO c5, 73 cells; VPS35 KO c7, 68 cells (means ± SEM; one-way ANOVA compared with parental HeLa. *, $P < 0.05$; **, $P < 0.01$; ***, $P < 0.001$; ****, $P < 0.001$).

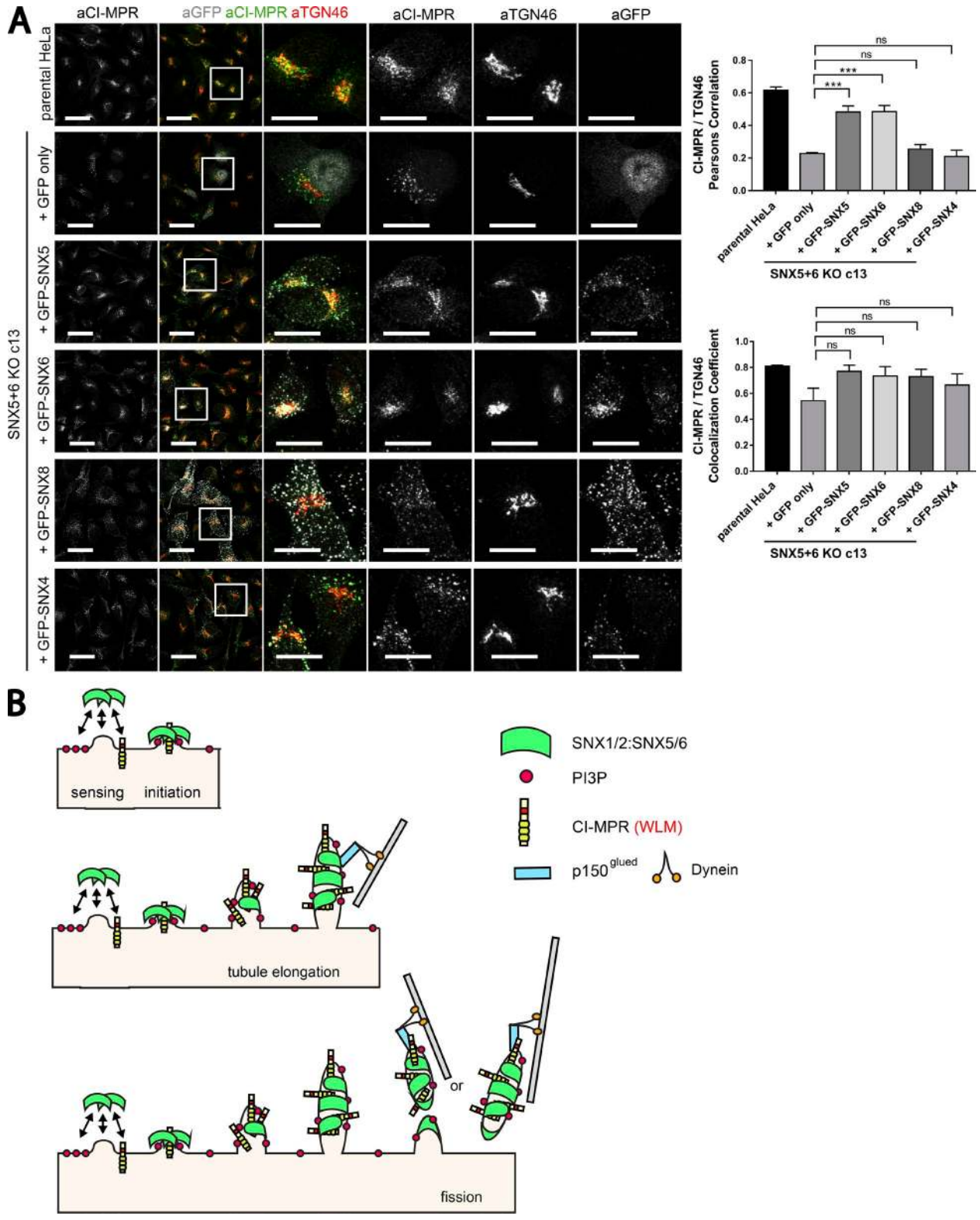

Figure 9. **Reexpression of GFP-tagged SNX5 or SNX6 rescues the normal steady-state distribution of CI-MPR in the SNX5+6 KO c13 clonal line.** (A) The SNX5+6 KO clonal line c13 was lentivirally transduced with GFP-SNX5, GFP-SNX6, GFP-SNX4, GFP-SNX8, or GFP alone. Colocalization analysis of endogenous CI-MPR and TGN marker TGN46 allowed comparison of CI-MPR distribution between the transduced lines and parental HeLa. Bars: (main images) 40 µm; (zooms) 20 µm. (A, right) $n = 3$ independent experiments; parental HeLa, 63 cells; +GFP, 70 cells; +SNX5, 72 cells; +SNX6, 78 cells; +SNX8, 66 cells; +SNX4, 73 cells (means ± SEM; one-way ANOVA compared with +GFP. ***, $P < 0.001$). (B) A schematic for how the SNX1/2–SNX5/6 complex coordinates sequence-dependent cargo recognition of the CI-MPR with the biogenesis of tubular-based cargo-enriched transport carriers.

References

Arighi, C.N., L.M. Hartnell, R.C. Aguilar, C.R. Haft, and J.S. Bonifacino. 2004. Role of the mammalian retromer in sorting of the cation-independent mannose 6-phosphate receptor. *J. Cell Biol.* 165:123–133. http://dx.doi.org/10.1083/jcb.200312055

Barbieri, M.A., G. Li, L.S. Mayorga, and P.D. Stahl. 1996. Characterization of Rab5:Q79L-stimulated endosome fusion. *Arch. Biochem. Biophys.* 326:64–72. http://dx.doi.org/10.1006/abbi.1996.0047

Bean, B.D., M. Davey, and E. Conibear. 2017. Cargo selectivity of yeast sorting nexins. *Traffic.* 18:110–122. http://dx.doi.org/10.1111/tra.12459

Burd, C., and P.J. Cullen. 2014. Retromer: a master conductor of endosome sorting. *Cold Spring Harb. Perspect. Biol.* 6:a016774. http://dx.doi.org/10.1101/cshperspect.a016774

Carlton, J., M. Bujny, B.J. Peter, V.M. Oorschot, A. Rutherford, H. Mellor, J. Klumperman, H.T. McMahon, and P.J. Cullen. 2004. Sorting nexin-1 mediates tubular endosome-to-TGN transport through coincidence sensing of high- curvature membranes and 3-phosphoinositides. *Curr. Biol.* 14:1791–1800. http://dx.doi.org/10.1016/j.cub.2004.09.077

Chen, C., D. Garcia-Santos, Y. Ishikawa, A. Seguin, L. Li, K.H. Fegan, G.J. Hildick-Smith, D.I. Shah, J.D. Cooney, W. Chen, et al. 2013. Snx3 regulates recycling of the transferrin receptor and iron assimilation. *Cell Metab.* 17:343–352. http://dx.doi.org/10.1016/j.cmet.2013.01.013

Collins, B.M., C.F. Skinner, P.J. Watson, M.N. Seaman, and D.J. Owen. 2005. Vps29 has a phosphoesterase fold that acts as a protein interaction scaffold for retromer assembly. *Nat. Struct. Mol. Biol.* 12:594–602. http://dx.doi.org/10.1038/nsmb954

Cullen, P.J. 2008. Endosomal sorting and signalling: an emerging role for sorting nexins. *Nat. Rev. Mol. Cell Biol.* 9:574–582. http://dx.doi.org/10.1038/nrm2427

Cullen, P.J., and H.C. Korswagen. 2011. Sorting nexins provide diversity for retromer-dependent trafficking events. *Nat. Cell Biol.* 14:29–37. http://dx.doi.org/10.1038/ncb2374

Dong, R., Y. Saheki, S. Swarup, L. Lucast, J.W. Harper, and P. De Camilli. 2016. Endosome-ER Contacts Control Actin Nucleation and Retromer Function through VAP-Dependent Regulation of PI4P. *Cell.* 166:408–423. http://dx.doi.org/10.1016/j.cell.2016.06.037

Fjorback, A.W., M. Seaman, C. Gustafsen, A. Mehmedbasic, S. Gokool, C. Wu, D. Militz, V. Schmidt, P. Madsen, J.R. Nyengaard, et al. 2012. Retromer binds the FANSHY sorting motif in SorLA to regulate amyloid precursor protein sorting and processing. *J. Neurosci.* 32:1467–1480. http://dx.doi.org/10.1523/JNEUROSCI.2272-11.2012

Freeman, C.L., G. Hesketh, and M.N. Seaman. 2014. RME-8 coordinates the activity of the WASH complex with the function of the retromer SNX dimer to control endosomal tubulation. *J. Cell Sci.* 127:2053–2070. http://dx.doi.org/10.1242/jcs.144659

Gallon, M., and P.J. Cullen. 2015. Retromer and sorting nexins in endosomal sorting. *Biochem. Soc. Trans.* 43:33–47. http://dx.doi.org/10.1042/BST20140290

Gallon, M., T. Clairfeuille, F. Steinberg, C. Mas, R. Ghai, R.B. Sessions, R.D. Teasdale, B.M. Collins, and P.J. Cullen. 2014. A unique PDZ domain and arrestin-like fold interaction reveals mechanistic details of endocytic recycling by SNX27-retromer. *Proc. Natl. Acad. Sci. USA.* 111:E3604–E3613. http://dx.doi.org/10.1073/pnas.1410552111

Ghosh, P., N.M. Dahms, and S. Kornfeld. 2003. Mannose 6-phosphate receptors: new twists in the tale. *Nat. Rev. Mol. Cell Biol.* 4:202–213. http://dx.doi.org/10.1038/nrm1050

Goldenring, J.R. 2015. Recycling endosomes. *Curr. Opin. Cell Biol.* 35:117–122. http://dx.doi.org/10.1016/j.ceb.2015.04.018

Gomez, T.S., and D.D. Billadeau. 2009. A FAM21-containing WASH complex regulates retromer-dependent sorting. *Dev. Cell.* 17:699–711. http://dx.doi.org/10.1016/j.devcel.2009.09.009

Haft, C.R., M. de la Luz Sierra, V.A. Barr, D.H. Haft, and S.I. Taylor. 1998. Identification of a family of sorting nexin molecules and characterization of their association with receptors. *Mol. Cell. Biol.* 18:7278–7287. http://dx.doi.org/10.1128/MCB.18.12.7278

Haft, C.R., M. de la Luz Sierra, R. Bafford, M.A. Lesniak, V.A. Barr, and S.I. Taylor. 2000. Human orthologs of yeast vacuolar protein sorting proteins Vps26, 29, and 35: assembly into multimeric complexes. *Mol. Biol. Cell.* 11:4105–4116. http://dx.doi.org/10.1091/mbc.11.12.4105

Harbour, M.E., S.Y. Breusegem, R. Antrobus, C. Freeman, E. Reid, and M.N. Seaman. 2010. The cargo-selective retromer complex is a recruiting hub for protein complexes that regulate endosomal tubule dynamics. *J. Cell Sci.* 123:3703–3717. http://dx.doi.org/10.1242/jcs.071472

Harbour, M.E., S.Y. Breusegem, and M.N. Seaman. 2012. Recruitment of the endosomal WASH complex is mediated by the extended 'tail' of Fam21 binding to the retromer protein Vps35. *Biochem. J.* 442:209–220. http://dx.doi.org/10.1042/BJ20111761

Harterink, M., F. Port, M.J. Lorenowicz, I.J. McGough, M. Silhankova, M.C. Betist, J.R.T. van Weering, R.G.H.P. van Heesbeen, T.C. Middelkoop, K. Basler, et al. 2011. A SNX3-dependent retromer pathway mediates retrograde transport of the Wnt sorting receptor Wntless and is required for Wnt secretion. *Nat. Cell Biol.* 13:914–923. http://dx.doi.org/10.1038/ncb2281

Heydorn, A., B.P. Søndergaard, B. Ersbøll, B. Holst, F.C. Nielsen, C.R. Haft, J. Whistler, and T.W. Schwartz. 2004a. A library of 7TM receptor C-terminal tails. Interactions with the proposed post-endocytic sorting proteins ERM-binding phosphoprotein 50 (EBP50), N-ethylmaleimide-sensitive factor (NSF), sorting nexin 1 (SNX1), and G protein-coupled receptor-associated sorting protein (GASP). *J. Biol. Chem.* 279:54291–54303. http://dx.doi.org/10.1074/jbc.M406169200

Heydorn, A., R.J. Ward, R. Jorgensen, M.M. Rosenkilde, T.M. Frimurer, G. Milligan, and E. Kostenis. 2004b. Identification of a novel site within G protein alpha subunits important for specificity of receptor-G protein interaction. *Mol. Pharmacol.* 66:250–259. http://dx.doi.org/10.1124/mol.66.2.250

Horazdovsky, B.F., B.A. Davies, M.N. Seaman, S.A. McLaughlin, S. Yoon, and S.D. Emr. 1997. A sorting nexin-1 homologue, Vps5p, forms a complex with Vps17p and is required for recycling the vacuolar protein-sorting receptor. *Mol. Biol. Cell.* 8:1529–1541. http://dx.doi.org/10.1091/mbc.8.8.1529

Huotari, J., and A. Helenius. 2011. Endosome maturation. *EMBO J.* 30:3481–3500. http://dx.doi.org/10.1038/emboj.2011.286

Jia, D., T.S. Gomez, D.D. Billadeau, and M.K. Rosen. 2012. Multiple repeat elements within the FAM21 tail link the WASH actin regulatory complex to the retromer. *Mol. Biol. Cell.* 23:2352–2361. http://dx.doi.org/10.1091/mbc.E11-12-1059

Kerr, M.C., J.S. Bennetts, F. Simpson, E.C. Thomas, C. Flegg, P.A. Gleeson, C. Wicking, and R.D. Teasdale. 2005. A novel mammalian retromer component, Vps26B. *Traffic.* 6:991–1001. http://dx.doi.org/10.1111/j.1600-0854.2005.00328.x

Kim, E., Y. Lee, H.J. Lee, J.S. Kim, B.S. Song, J.W. Huh, S.R. Lee, S.U. Kim, S.H. Kim, Y. Hong, et al. 2010. Implication of mouse Vps26b-Vps29-Vps35 retromer complex in sortilin trafficking. *Biochem. Biophys. Res. Commun.* 403:167–171. http://dx.doi.org/10.1016/j.bbrc.2010.10.121

Kurten, R.C., D.L. Cadena, and G.N. Gill. 1996. Enhanced degradation of EGF receptors by a sorting nexin, SNX1. *Science.* 272:1008–1010. http://dx.doi.org/10.1126/science.272.5264.1008

Lombardi, D., T. Soldati, M.A. Riederer, Y. Goda, M. Zerial, and S.R. Pfeffer. 1993. Rab9 functions in transport between late endosomes and the trans Golgi network. *EMBO J.* 12:677–682.

Lucas, M., D.C. Gershlick, A. Vidaurrazaga, A.L. Rojas, J.S. Bonifacino, and A. Hierro. 2016. Structural Mechanism for Cargo Recognition by the Retromer Complex. *Cell.* 167:1623–1635.

Ma, M., C.G. Burd, and R.J. Chi. 2017. Distinct complexes of yeast Snx4 family SNX-BARs mediate retrograde trafficking of Snc1 and Atg27. *Traffic.* 18:134–144. http://dx.doi.org/10.1111/tra.12462

Maxfield, F.R., and T.E. McGraw. 2004. Endocytic recycling. *Nat. Rev. Mol. Cell Biol.* 5:121–132. http://dx.doi.org/10.1038/nrm1315

McGough, I.J., F. Steinberg, M. Gallon, A. Yatsu, N. Ohbayashi, K.J. Heesom, M. Fukuda, and P.J. Cullen. 2014a. Identification of molecular heterogeneity in SNX27-retromer-mediated endosome-to-plasma-membrane recycling. *J. Cell Sci.* 127:4940–4953. http://dx.doi.org/10.1242/jcs.156299

McGough, I.J., F. Steinberg, D. Jia, P.A. Barbuti, K.J. McMillan, K.J. Heesom, A.L. Whone, M.A. Caldwell, D.D. Billadeau, M.K. Rosen, and P.J. Cullen. 2014b. Retromer binding to FAM21 and the WASH complex is perturbed by the Parkinson disease-linked VPS35(D620N) mutation. *Curr. Biol.* 24:1670–1676. (published erratum can be found in *Curr. Biol.* 24:1678) http://dx.doi.org/10.1016/j.cub.2014.06.024

McMillan, K.J., M. Gallon, A.P. Jellett, T. Clairfeuille, F.C. Tilley, I. McGough, C.M. Danson, K.J. Heesom, K.A. Wilkinson, B.M. Collins, and P.J. Cullen. 2016. Atypical parkinsonism-associated retromer mutant alters endosomal sorting of specific cargo proteins. *J. Cell Biol.* 214:389–399. http://dx.doi.org/10.1083/jcb.201604057

Meyer, C., D. Zizioli, S. Lausmann, E.L. Eskelinen, J. Hamann, P. Saftig, K. von Figura, and P. Schu. 2000. mu1A-adaptin-deficient mice: lethality, loss of AP-1 binding and rerouting of mannose 6-phosphate receptors. *EMBO J.* 19:2193–2203. http://dx.doi.org/10.1093/emboj/19.10.2193

Murk, J.L., B.M. Humbel, U. Ziese, J.M. Griffith, G. Posthuma, J.W. Slot, A.J. Koster, A.J. Verkleij, H.J. Geuze, and M.J. Kleijmeer. 2003. Endosomal compartmentalization in three dimensions: implications for

membrane fusion. *Proc. Natl. Acad. Sci. USA.* 100:13332–13337. http://dx.doi.org/10.1073/pnas.2232379100

Norris, A., P. Tammineni, S. Wang, J. Gerdes, A. Murr, K.Y. Kwan, Q. Cai, and B.D. Grant. 2017. SNX-1 and RME-8 oppose the assembly of HGRS-1/ESCRT-0 degradative microdomains on endosomes. *Proc. Natl. Acad. Sci. USA.* 114:E307–E316. http://dx.doi.org/10.1073/pnas.1612730114

Norwood, S.J., D.J. Shaw, N.P. Cowieson, D.J. Owen, R.D. Teasdale, and B.M. Collins. 2011. Assembly and solution structure of the core retromer protein complex. *Traffic.* 12:56–71. http://dx.doi.org/10.1111/j.1600-0854.2010.01124.x

Parks, W.T., D.B. Frank, C. Huff, C. Renfrew Haft, J. Martin, X. Meng, M.P. de Caestecker, J.G. McNally, A. Reddi, S.I. Taylor, et al. 2001. Sorting nexin 6, a novel SNX, interacts with the transforming growth factor-beta family of receptor serine-threonine kinases. *J. Biol. Chem.* 276:19332–19339. http://dx.doi.org/10.1074/jbc.M100606200

Peters, C., T.L. Baars, S. Bühler, and A. Mayer. 2004. Mutual control of membrane fission and fusion proteins. *Cell.* 119:667–678. http://dx.doi.org/10.1016/j.cell.2004.11.023

Popoff, V., G.A. Mardones, S.-K. Bai, V. Chambon, D. Tenza, P.V. Burgos, A. Shi, P. Benaroch, S. Urbé, C. Lamaze, et al. 2009. Analysis of articulation between clathrin and retromer in retrograde sorting on early endosomes. *Traffic.* 10:1868–1880. http://dx.doi.org/10.1111/j.1600-0854.2009.00993.x

Puthenveedu, M.A., B. Lauffer, P. Temkin, R. Vistein, P. Carlton, K. Thorn, J. Taunton, O.D. Weiner, R.G. Parton, and M. von Zastrow. 2010. Sequence-dependent sorting of recycling proteins by actin-stabilized endosomal microdomains. *Cell.* 143:761–773. http://dx.doi.org/10.1016/j.cell.2010.10.003

Raiborg, C., K.G. Bache, D.J. Gillooly, I.H. Madshus, E. Stang, and H. Stenmark. 2002. Hrs sorts ubiquitinated proteins into clathrin-coated microdomains of early endosomes. *Nat. Cell Biol.* 4:394–398. http://dx.doi.org/10.1038/ncb791

Rojas, R., S. Kametaka, C.R. Haft, and J.S. Bonifacino. 2007. Interchangeable but essential functions of SNX1 and SNX2 in the association of retromer with endosomes and the trafficking of mannose 6-phosphate receptors. *Mol. Cell. Biol.* 27:1112–1124. http://dx.doi.org/10.1128/MCB.00156-06

Schöneberg, J., I.H. Lee, J.H. Iwasa, and J.H. Hurley. 2017. Reverse-topology membrane scission by the ESCRT proteins. *Nat. Rev. Mol. Cell Biol.* 18:5–17. http://dx.doi.org/10.1038/nrm.2016.121

Seaman, M.N. 2004. Cargo-selective endosomal sorting for retrieval to the Golgi requires retromer. *J. Cell Biol.* 165:111–122. http://dx.doi.org/10.1083/jcb.200312034

Seaman, M.N. 2007. Identification of a novel conserved sorting motif required for retromer-mediated endosome-to-TGN retrieval. *J. Cell Sci.* 120:2378–2389. http://dx.doi.org/10.1242/jcs.009654

Seaman, M.N., J.M. McCaffery, and S.D. Emr. 1998. A membrane coat complex essential for endosome-to-Golgi retrograde transport in yeast. *J. Cell Biol.* 142:665–681. http://dx.doi.org/10.1083/jcb.142.3.665

Shi, A., L. Sun, R. Banerjee, M. Tobin, Y. Zhang, and B.D. Grant. 2009. Regulation of endosomal clathrin and retromer-mediated endosome to Golgi retrograde transport by the J-domain protein RME-8. *EMBO J.* 28:3290–3302. http://dx.doi.org/10.1038/emboj.2009.272

Simunovic, M., and G.A. Voth. 2015. Membrane tension controls the assembly of curvature-generating proteins. *Nat. Commun.* 6:7219. http://dx.doi.org/10.1038/ncomms8219

Sönnichsen, B., S. De Renzis, E. Nielsen, J. Rietdorf, and M. Zerial. 2000. Distinct membrane domains on endosomes in the recycling pathway visualized by multicolor imaging of Rab4, Rab5, and Rab11. *J. Cell Biol.* 149:901–914. http://dx.doi.org/10.1083/jcb.149.4.901

Steinberg, F., M. Gallon, M. Winfield, E.C. Thomas, A.J. Bell, K.J. Heesom, J.M. Tavaré, and P.J. Cullen. 2013. A global analysis of SNX27-retromer assembly and cargo specificity reveals a function in glucose and metal ion transport. *Nat. Cell Biol.* 15:461–471. http://dx.doi.org/10.1038/ncb2721

Strochlic, T.I., T.G. Setty, A. Sitaram, and C.G. Burd. 2007. Grd19/Snx3p functions as a cargo-specific adapter for retromer-dependent endocytic recycling. *J. Cell Biol.* 177:115–125. http://dx.doi.org/10.1083/jcb.200609161

Tabuchi, M., I. Yanatori, Y. Kawai, and F. Kishi. 2010. Retromer-mediated direct sorting is required for proper endosomal recycling of the mammalian iron transporter DMT1. *J. Cell Sci.* 123:756–766. http://dx.doi.org/10.1242/jcs.060574

Teasdale, R.D., and B.M. Collins. 2012. Insights into the PX (phox-homology) domain and SNX (sorting nexin) protein families: structures, functions and roles in disease. *Biochem. J.* 441:39–59. http://dx.doi.org/10.1042/BJ20111226

Temkin, P., B. Lauffer, S. Jäger, P. Cimermancic, N.J. Krogan, and M. von Zastrow. 2011. SNX27 mediates retromer tubule entry and endosome-to-plasma membrane trafficking of signalling receptors. *Nat. Cell Biol.* 13:715–721. http://dx.doi.org/10.1038/ncb2252

Traer, C.J., A.C. Rutherford, K.J. Palmer, T. Wassmer, J. Oakley, N. Attar, J.G. Carlton, J. Kremerskothen, D.J. Stephens, and P.J. Cullen. 2007. SNX4 coordinates endosomal sorting of TfnR with dynein-mediated transport into the endocytic recycling compartment. *Nat. Cell Biol.* 9:1370–1380. http://dx.doi.org/10.1038/ncb1656

van Weering, J.R., and P.J. Cullen. 2014. Membrane-associated cargo recycling by tubule-based endosomal sorting. *Semin. Cell Dev. Biol.* 31:40–47. http://dx.doi.org/10.1016/j.semcdb.2014.03.015

van Weering, J.R., R.B. Sessions, C.J. Traer, D.P. Kloer, V.K. Bhatia, D. Stamou, S.R. Carlsson, J.H. Hurley, and P.J. Cullen. 2012a. Molecular basis for SNX-BAR-mediated assembly of distinct endosomal sorting tubules. *EMBO J.* 31:4466–4480. http://dx.doi.org/10.1038/emboj.2012.283

van Weering, J.R., P. Verkade, and P.J. Cullen. 2012b. SNX-BAR-mediated endosome tubulation is co-ordinated with endosome maturation. *Traffic.* 13:94–107. http://dx.doi.org/10.1111/j.1600-0854.2011.01297.x

Villar, V.A., I. Armando, H. Sanada, L.C. Frazer, C.M. Russo, P.M. Notario, H. Lee, L. Comisky, H.A. Russell, Y. Yang, et al. 2013. Novel role of sorting nexin 5 in renal D(1) dopamine receptor trafficking and function: implications for hypertension. *FASEB J.* 27:1808–1819. http://dx.doi.org/10.1096/fj.12-208439

Waguri, S., F. Dewitte, R. Le Borgne, Y. Rouillé, Y. Uchiyama, J.F. Dubremetz, and B. Hoflack. 2003. Visualization of TGN to endosome trafficking through fluorescently labeled MPR and AP-1 in living cells. *Mol. Biol. Cell.* 14:142–155. http://dx.doi.org/10.1091/mbc.E02-06-0338

Wassmer, T., N. Attar, M.V. Bujny, J. Oakley, C.J. Traer, and P.J. Cullen. 2007. A loss-of-function screen reveals SNX5 and SNX6 as potential components of the mammalian retromer. *J. Cell Sci.* 120:45–54. http://dx.doi.org/10.1242/jcs.03302

Wassmer, T., N. Attar, M. Harterink, J.R. van Weering, C.J. Traer, J. Oakley, B. Goud, D.J. Stephens, P. Verkade, H.C. Korswagen, and P.J. Cullen. 2009. The retromer coat complex coordinates endosomal sorting and dynein-mediated transport, with carrier recognition by the trans-Golgi network. *Dev. Cell.* 17:110–122. http://dx.doi.org/10.1016/j.devcel.2009.04.016